

A MATHEMATICAL SIMULATION OF THE PYROLYSIS OF A MODEL ASPHALTENE

PHILLIP E. SAVAGE¹ AND MICHAEL T. KLEIN

DEPARTMENT OF CHEMICAL ENGINEERING
AND
CENTER FOR CATALYTIC SCIENCE AND TECHNOLOGY
UNIVERSITY OF DELAWARE
NEWARK, DE 19716

¹ PRESENT ADDRESS: UNIVERSITY OF MICHIGAN
DEPARTMENT OF CHEMICAL ENGINEERING
ANN ARBOR, MI 48109

INTRODUCTION

Reaction engineering experiments with coal or heavy oil fractions typically allow observation of only global kinetics and the yields of lumped product fractions; the controlling reaction fundamentals are obscured by the complexity of the reactant and its product spectra. This limitation has motivated experiments with model compounds to help resolve the fundamental reaction pathways, kinetics, and mechanisms involved. These fundamentals are of the model compound reactions, however, and their relation to the reactions of the moieties they mimic in a complex reactant can be vague. Model compound results are often used in the analysis of the reactions of coal or asphaltenes in a qualitative fashion. The object of this paper is to report on a mathematical model of asphaltene pyrolysis which serves as a quantitative bridge between model compounds and actual asphaltenes by combining model-compound deduced reaction pathways and kinetics with aspects of asphaltene structure.

BACKGROUND

Asphaltenes are operationally defined as a response to a solvent extraction protocol. However, the functional groups and chemical moieties they comprise have been probed by numerous spectroscopic and pyrolytic investigations (1-5), and structural scenarios typically include condensed aromatic and heteroaromatic cores to which are attached peripheral alkyl, naphthenic, and heteroatomic substituents. Several of these substituted aromatic cores, referred to as unit sheets, can be bonded together in macromolecular fashion to form an asphaltene particle.

Of the covalent bonds in asphaltene, those in heteroatomic peripheral substituents are the most thermally labile; they are also present in relatively low proportions. C-C bonds in aromatic rings, on the other hand, constitute a large fraction of asphaltene bonds, but they are stable even at very high temperatures. Aliphatic C-C bonds in alkyaromatic, alkyhydroaromatic, and alkylnaphthenic positions are both abundant and reactive and thus constitute the most prevalent thermally scissile groups in asphaltene. Therefore, the reactions (6-10) of the model compounds n-pentadecylbenzene, n-dodecylbenzene, n-butylbenzene, 2-ethylnaphthalene, n-tridecylcyclohexane, and 2-ethyltetralin, mimics of these scissile moieties, seemed a relevant probe of the thermal reactions of the basic hydrocarbon framework of asphaltenes. These model compound data were combined with asphaltene structural information to simulate the pyrolysis of a generic, hypothetical, fully hydrocarbon asphaltene. Structural data used in the model were selected from an overall understanding of asphaltene composition and constitution (8) and were not obtained from spectroscopic characterization of any particular asphaltene. Note however, that the model can readily incorporate structural data from any asphaltene of interest and simulate its pyrolysis specifically.

MODEL DEVELOPMENT

Reactant Asphaltene.

The simulated asphaltene is illustrated schematically in Figure 1. Asphaltenes were regarded (8) as a blend of hydrocarbon particles, defined as covalently bonded oligomers of unit sheets with a degree of polymerization ranging from 1 to 5. The unit sheets comprised between 2 and 30 six-membered rings which could, in turn, be either aromatic or saturated. The maximum number of aromatic rings in a unit sheet was 15, and the number of

saturated rings never exceeded the number of aromatic rings. Peripheral aromatic and saturated carbon atoms in a unit sheet were, respectively, 45% and 25% substituted by aliphatic chains containing from 1 to 25 carbon atoms. A fraction of these chains served as the covalent links which bonded unit sheets into particles, and the balance were terminal substituents.

Four probability distributions describing, respectively, the alkyl substituent chain lengths, the number of aromatic and the number of saturated rings in a unit sheet, and the degree of polymerization of asphaltene particles are displayed in Figure 2. These data were selected such that the average structural parameters for the reactant asphaltene were consistent with values reported in the literature.

In the simulations, the reactant asphaltene consisted of a collection of particles containing the model's basis of 10,000 unit sheets, assembled in a stochastic process. The first step of this assembly was to determine the number of unit sheets in each particle by comparing a random number between 0 and 1 with the integrated probability distribution describing the particle's degree of polymerization (i.e. Fig 2d). The numbers of aromatic and saturated rings in each of the unit sheets in the particle were then determined by comparing independent random numbers with the integrated probability distributions in Figures 2b and 2c. Each saturated ring in the unit sheet was then individually categorized as either hydroaromatic or naphthenic based on whether it was fused to an aromatic ring or exclusively to other saturated rings, respectively. This was accomplished by comparing a random number with the probability, P_H , of a saturated ring being fused to an aromatic ring. P_H was estimated from Equation 1 on the basis that the type of ring (saturated or aromatic) to which a saturated ring was fused was directly proportional to the number of aromatic, N_{ar} , or saturated, N_{nr} , rings in the unit sheet.

$$P_H = \frac{N_{ar}}{N_{ar} + N_{nr} - 1} \quad (1)$$

The numbers of internal and peripheral aromatic and saturated carbon atoms in the unit sheet, defined respectively as those bonded to 3 and to 2 other cyclic carbon atoms, were calculated according to the method of Hirsch and Altgelt (11,12). The number of peripheral atoms of each type was then multiplied by their appropriate degrees of substitution (0.45 and 0.25 for aromatic and saturated carbons, respectively) to calculate the number of peripheral positions containing substituents. The number of peripheral aromatic carbon atoms bearing alkyl chains was then calculated as the total number of substituted aromatic carbon atoms minus the number of peripheral aromatic carbon atoms in hydroaromatic rings. Assembly of the unit sheets was finally completed by comparing a random number with the integrated probability distribution in Figure 2a to determine the number of carbon atoms in each aliphatic substituent. The steps outlined above were repeated for each unit sheet until an entire particle had been constructed. Additional particles were then assembled until 10,000 unit sheets had been included.

Pyrolysis Simulation.

The model compound pyrolyses (8) revealed that ring-opening reactions were of minor consequence for even the saturated rings. Therefore, the polycyclic portion of the unit sheet was modeled as being thermally stable and, hence, conserved during pyrolysis. The only effect of pyrolysis was then to break C-C bonds in the peripheral alkyl substituents and the inter-unit sheet links.

Asphaltene pyrolysis therefore amounted to accounting for the temporal variation of the distribution functions of Figure 2. This was accomplished by 1.) developing differential rate equations for the three reactive moieties (i.e. alkylaromatic, alkyl-naphthenic, and alkylhydroaromatic), 2.) integrating these equations numerically with model-compound-deduced rate constants as parameters, 3.) updating the integrated probability distributions to reflect the effects of pyrolysis, and 4.) using the updated distributions to stochastically assemble 10,000 unit sheets which represented the reaction products.

The rate of reaction of an alkylaromatic chain, A_i , of length i in a constant-volume batch reactor was given as Equation 2 where k_{A_i} is the first-order rate constant.

$$\frac{dA_i}{dt} = -k_{A_i} A_i + \sum_{j=1}^{25-i} \nu_{A_{i+j}, i} k_{A_{i+j}} A_{i+j} \quad (2)$$

The two terms on the right hand side account for, respectively, the cleavage of alkylaromatic substituents with i carbon atoms, and the formation of alkylaromatics with i carbons from alkylaromatics containing $i+j$ carbon

atoms where $\nu_{A_{i+j}}$ is the stoichiometric coefficient. Completely analogous equations described the rate of reaction of the alkylnaphthenic, N_i , and alkyhydroaromatic, H_i , moieties.

The rate of formation of aliphatic products, AP_i , with i carbon atoms is given by Equation 3, where k and ν are rate constants and stoichiometric coefficients, respectively. Note that secondary reactions of the primary aliphatic products were neglected.

$$\frac{dAP_i}{dt} = \sum_{j=1}^{25-i} (\nu_{A_{i+j,j}} k_{A_{i+j}} A_{i+j} + \nu_{H_{i+j,j}} k_{H_{i+j}} H_{i+j} + \nu_{N_{i+j,j}} k_{N_{i+j}} N_{i+j}) \quad (3)$$

Finally, cleavage of the inter-unit sheet links in the oligomeric particles was described by Equation 4. In modeling the depolymerization kinetics, all inter-unit sheet linkages were treated as alkyaromatic chains. That is, the rate constant for breaking an inter-unit link was the same as that for cleaving an alkyaromatic substituent.

$$\frac{dP_i}{dt} = -k_{A_i} P_i (i-1) + \sum_{j=1}^{5-i} 2k_{A_{i+j}} P_{i+j} \quad (4)$$

The two terms on the right hand side account for the depolymerization of particles containing i unit sheets, P_i , and the formation of such particles from those with more than i unit sheets, P_{i+j} , respectively.

The rate constants and stoichiometric coefficients required for numerical solution of Equations 2-4 were obtained from the model compound pyrolyses (6-9). For example, the initial product selectivities in pentadecylbenzene (PDB) pyrolysis (6,9) showed that bond scission occurred at the β position about 35% of the time, at the γ position 15% of the time, and at each of the other 12 bonds roughly 4% of the time. These relative proportions for cleavage of each aliphatic bond were modelled to apply to all other alkyaromatics. Similarly, the initial selectivities observed for tridecylcyclohexane (TDC) and 2-ethyltetralin (2ET) pyrolyses (8) provided the stoichiometric coefficients for the alkylnaphthenic and alkyhydroaromatic moieties, respectively.

A unique rate constant for each of the 3 reactive moieties containing from 1 to 25 aliphatic carbons was calculated from the rate constant for the relevant model compound scaled by the square root of the carbon number, as suggested by the apparent first-order rate constant for a Rice-Herzfeld (13) chain. For example, all 15 carbon atom alkyaromatic chains were assumed to follow the pyrolysis kinetics of PDB, and rate constants for alkyaromatic chains with i carbon atoms were calculated as

$$k_{A_i} = k_{PDB} \left(\frac{i}{15}\right)^{1/2} \quad (5)$$

Although only approximate, Equation 5 correlated available experimental data quite well (8).

To summarize, this mathematical model simulated asphaltene pyrolysis by simultaneously solving 105 differential rate equations; 25 each for cleavage of alkyaromatic, alkylnaphthenic, and alkyhydroaromatic moieties, 25 for the formation of aliphatic products, and 5 for depolymerization of asphaltene particles. The kinetic parameters in these equations were deduced through model compound pyrolyses. The structural data in the probability distributions, shown in Figure 2 for the reactant asphaltene, were then updated to reflect the effects of pyrolysis, and 10,000 unit sheets were assembled as reaction products.

Reaction Products.

The simulated pyrolyses produced aliphatics, via scission of peripheral moieties on the asphaltenic unit sheet, and product particles containing at least one unit sheet. The product particles were stochastically assembled using the procedure described previously for the reactant asphaltene particles, and they differed from their precursors only in their degree of polymerization and in the length and number of their terminal aliphatic constituents. The polycyclic portion of the unit sheet was thermally stable and hence unaltered by pyrolysis.

To allow comparison with experimentally observed (9,10) temporal variations of solubility-based product fractions from asphaltene pyrolysis, each reaction product from the simulated pyrolyses was assigned to either a gas, maltene, asphaltene, or coke product fraction. Aliphatic products were assigned to the gas fraction if they contained 4 or fewer carbon atoms and to the maltene fraction if they contained more than 4 carbon atoms. The product particles were assigned to one of the solubility-based product fractions on the basis of combinations

of molecular weight and H/C atomic ratio as shown in Table 1. These two parameters provided a physically significant yet convenient means of correlating particle solubility with chemical composition and structure in this model.

MODEL RESULTS

The simulations were of the constant-volume, isothermal, batch pyrolyses of a generic asphaltene and not the particular off-shore California asphaltene used in the experiments. Quantitative agreement between the model and experimental results should not be expected in all cases and treated as a coincidence when found. Note that detailed spectroscopic analysis of any one asphaltene could permit prediction of its reactions, however. Model predictions are presented in terms of the temporal variation of average structural parameters and solubility-based product fractions.

Structural Parameters.

The model monitored the number of each type of aliphatic, aromatic, and naphthenic carbon and hydrogen atoms in the 10,000 unit sheets so that average structural parameters could be determined for the collection of asphaltene particles. The values of selected structural parameters for the reactant asphaltene are reported in Table 2 and are clearly consistent with the ranges of these parameters typically reported in the literature (2,3,14-19) for petroleum asphaltenes.

Figure 3 presents the temporal variation of the particle and unit sheet number average molecular weights, whereas Figure 4 displays the particle molecular weight distribution parameteric in time for simulated asphaltene pyrolysis at 425°C. The particle molecular weight decreased very rapidly and approached the unit sheet average molecular weight, suggesting essentially complete asphaltene depolymerization. Figure 4 shows that the molecular weight distribution for the reactant asphaltene was broad and possessed a high average value and that a significant reduction in average molecular weight and a narrowing of the distribution occurred for asphaltene pyrolysis even at short reaction times.

Experimental data are lacking for a direct quantitative comparison of the model results in Figures 3 and 4, but previous experiments (8) do allow limited scrutiny as follows. Asphaltene pyrolyses at 400°C for 30 min significantly reduced the average molecular weight of the sulfur- and vanadium-containing compounds in asphaltene and shifted the molecular weight distribution to lower values. These results, if generally true for all of the asphaltenic constituents, are in qualitative accord with the model's predictions.

The temporal variation of the H/C atomic ratio and the fraction of carbon atoms being aromatic, f_a , from simulated asphaltene pyrolyses at 425°C are portrayed on Figure 5. The H/C atomic ratio decreased from 1.20 initially to 0.85 at 120 min. The value of f_a , on the other hand, increased from an initial value of 0.42 to 0.61 at 120 min. The predicted variation of the H/C ratio is in good accord with the experimental results from asphaltene pyrolysis at 400°C shown in Figure 6. No experimental data were available for comparison with the temporal variation of f_a .

Product Fractions.

Figure 7 presents the temporal variations of the yields of the gas, maltene, asphaltene, and coke product fractions from simulated asphaltene pyrolyses at 400, 425, and 450°C. Experimental data are provided in Figure 8 for comparison. The simulations at 400°C predicted the experimentally observed induction period for coke production, and maltene and gas yields of the correct order. No experiments were performed at 425°C, but the results of simulated pyrolyses at this temperature closely resembled the experimental results at 400°C. This corroborates the qualitative trends predicted by the model, and further suggests that the model of a generic asphaltene underpredicted the reactivity of the off-shore California asphaltene used in the experiments. The agreement between the model predictions and the experimental temporal variations of the product fractions at 450°C was almost quantitative. Essentially complete asphaltene conversion at 30 minutes, an ultimate coke yield of about 60% that decreased with time, and an ultimate yield of maltenes and gases of about 40% are all common features.

DISCUSSION

The model predictions were consistent with the available experimental data on a qualitative basis without exception, and on a quantitative basis in several instances. This agreement between model and experimental

results is striking because the model deals with a simplified asphaltene structure, includes only model-compound-deduced reaction pathways and kinetics, and contains no kinetics parameters regressed from experiments with actual asphaltenes. The overall consistency of the experimental and simulated asphaltene pyrolyses suggest that the model included many key features of asphaltene structure and its thermal reactivity, and that the pyrolysis kinetics of the model compounds mimicked those of the related moieties in asphaltene.

The model results showed that dealkylation of the asphaltene unit sheets caused the particles to become increasingly hydrogen deficient and more aromatic thereby suggesting an attendant change in their toluene-solubility. Thus as reactant asphaltenes, toluene soluble because of their aliphaticity, were cleaved of their peripheral substituents their toluene solubility diminished, and they eventually appeared as coke in the pyrolysis simulation. The modeling results thus demonstrate that severe overreaction of primary products is not necessary to predict high yields of coke. This corroborates our previous interpretation (10) of the coke fraction as, mainly, a primary pyrolysis product containing the polycyclic cores of asphaltenic unit sheets.

Finally, the model results also permit speculation into the role of pyrolysis in nominally catalytic asphaltene hydroprocessing reactions. The simulations showed that asphaltene depolymerization occurred even at short reaction times and that many particles existed as single unit sheets rather than covalently bonded oligomers thereof. These individual asphaltene unit sheets, which are much smaller than the macromolecular particles, will be major participants in catalytic reactions because they can more readily diffuse within the porous catalyst. This suggests that catalytic hydroprocessing at high temperatures will be of thermally derived asphaltene fragments and not the asphaltene particle itself.

LITERATURE CITED

- 1 Yen, T. F. in Chemistry of Asphaltenes, ACS Adv. Chem. Ser. No. 195 1981, 39.
- 2 Yen, T. F., Wu, W. H., Chilingar, G. V. *Energy Sources* 1984, 7, 203.
- 3 Yen, T. F., Wu, W. H., Chilingar, G. V. *Energy Sources* 1984, 7, 275.
- 4 Speight, J. G., Moschopedis, S. E. in Chemistry of Asphaltenes, ACS Adv. Chem. Ser. No. 195 1981, 1.
- 5 Koots, J. A., Speight, J. G. *Fuel* 1975, 54, 179.
- 6 Savage, P. E., Klein, M. T. *Ind. Eng. Chem. Research* 1987, in press.
- 7 Savage, P. E., Klein, M. T. *Ind. Eng. Chem. Research* 1987, 26, 374.
- 8 Savage, P. E. *Ph.D. Dissertation* University of Delaware 1986
- 9 Savage, P. E., Klein, M. T., Kukes, S. G. *ACS Div. Fuel Chem. Prepr.* 1985 30, 408.
- 10 Savage, P. E., Klein, M. T., Kukes, S. G. *Ind. Eng. Chem. Process Des. Dev.* 1985, 24, 1169.
- 11 Hirsch, E., Altgelt, K. H. *Anal. Chem.* 1970, 42, 1330.
- 12 Hirsch, E. *Anal. Chem.* 1970, 42, 1326.
- 13 Rice, F. O., Herzfeld, K. F. *J. Am. Chem. Soc.* 1934, 56, 284.
- 14 Ali, L. H., Al-Ghannam, K. A. *Fuel* 1981, 60, 1043.
- 15 Boduszynski, M. M., Chadha, B. R., Szkuta-Pochopien, T. *Fuel* 1977, 56, 443.
- 16 Speight, J. G. *Fuel* 1970, 49, 134.
- 17 Speight, J. G. *Fuel* 1971, 50, 102.
- 18 Suzuki, T., Itoh, M., Takegami, Y., Watanabe, Y. *Fuel* 1982, 61, 402.
- 19 Yen, T. F. *Energy Sources* 1974, 1, 447.

TABLE ONE
CRITERIA FOR ASSIGNING PARTICLES TO PRODUCT FRACTIONS

<u>Criteria</u>	<u>Product Fraction</u>	<u>Operational Definition</u>
MW < 300 and H/C > 1.0	Maltene	heptane - soluble
MW > 300 and H/C > 1.0	Asphaltene	heptane - insoluble
MW < 300 and H/C < 1.0		toluene - soluble
MW > 300 and H/C < 1.0	Coke	toluene - insoluble

TABLE TWO
AVERAGE STRUCTURAL PARAMETERS FOR PETROLEUM ASPHALTENE

<u>Parameter</u>	<u>Significance</u>	<u>Model</u>	<u>Literature (1-5, 14-19)</u>
H/C	atomic ratio	1.20	1.09 - 1.29
f_a	fraction of C atoms in aromatic rings	0.42	0.30 - 0.61
f_n	fraction of C atoms in saturated rings	0.13	0.06 - 0.24
H_a	fraction of H atoms in aromatic rings	0.09	0.04 - 0.11
H_n	fraction of H atoms in saturated rings	0.16	0.16 - 0.19
C_p/C_a	<u>peripheral aromatic carbons</u> total aromatic carbons (shape of aromatic core)	0.48	0.31 - 0.55
C_s/C_{sa}	<u>total saturated carbons</u> saturated carbons α to ring (average alkyl chain length)	4.93	3.1 - 8.4
C_{sa}/C_p	<u>saturated carbons α to ring</u> peripheral aromatic carbons (degree of substitution of aromatics in unit sheet)	0.45	0.39 - 0.65

Figure 1: Structural Hierarchy in Pyrolysis Model

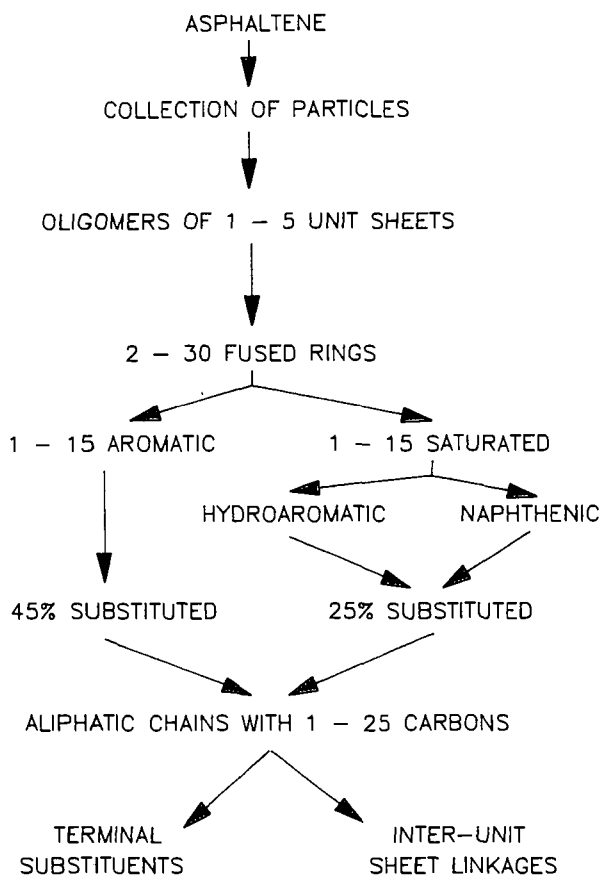


Figure 2: Integrated Distributions for Elements of Asphaltene Structure

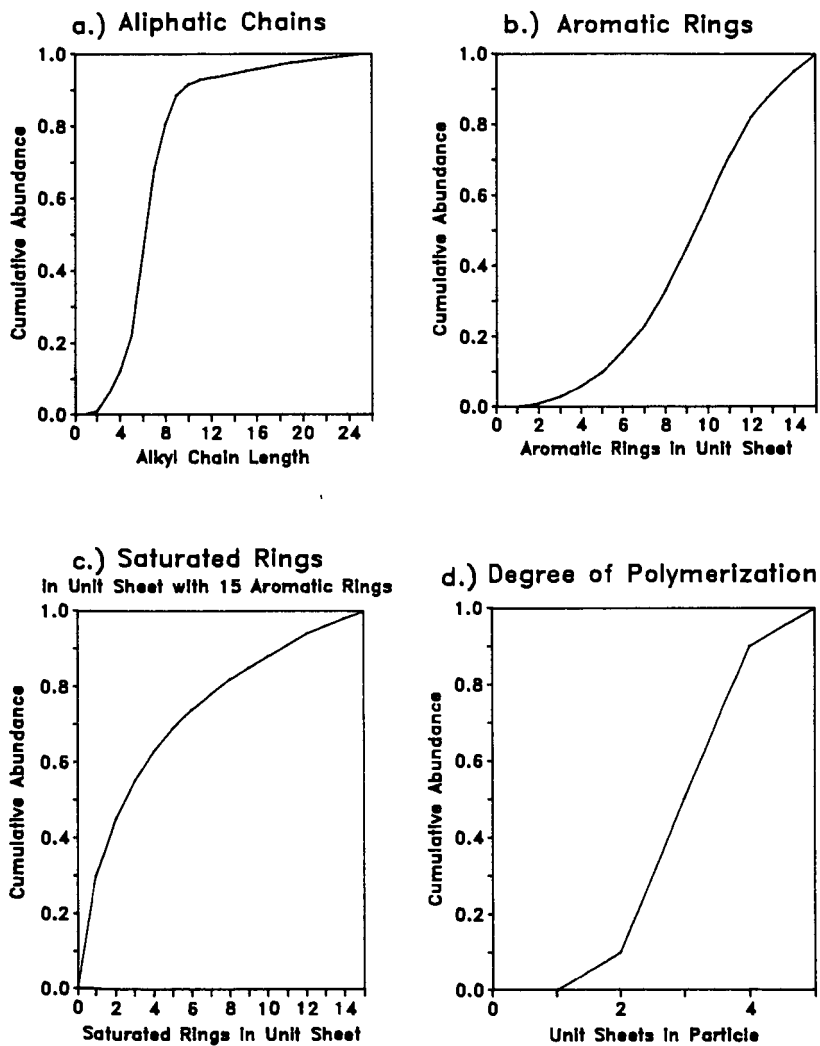


Figure 3: Temporal Variation of MW
SIMULATED PYROLYSIS AT 425C

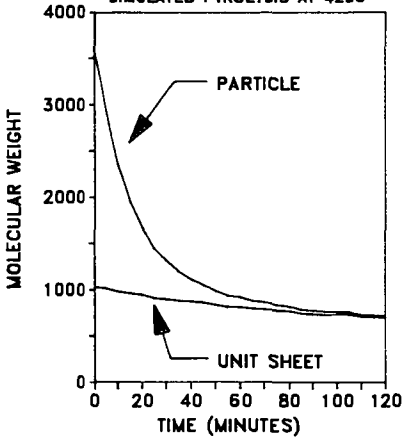


Figure 4: Molecular Weight Distributions
SIMULATED PYROLYSIS AT 425C

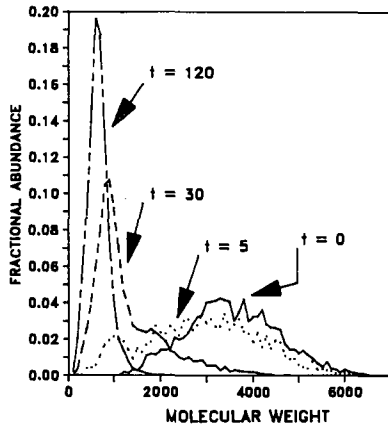


Figure 5: Temporal Variation of H/C and f_a
SIMULATED PYROLYSIS AT 425C

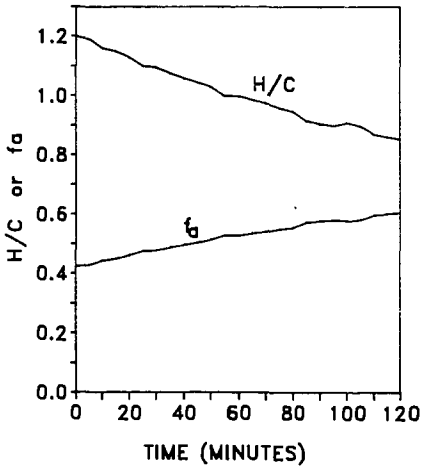


Figure 6: Temporal Variation of H/C
ASPHALTENE PYROLYSIS AT 400C

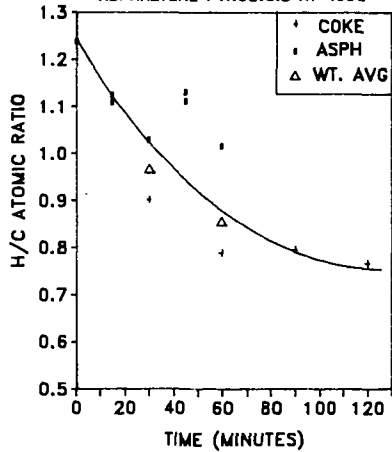


Figure 7: Temporal Variation of Product Fractions from Simulated Asphaltene Pyrolysis

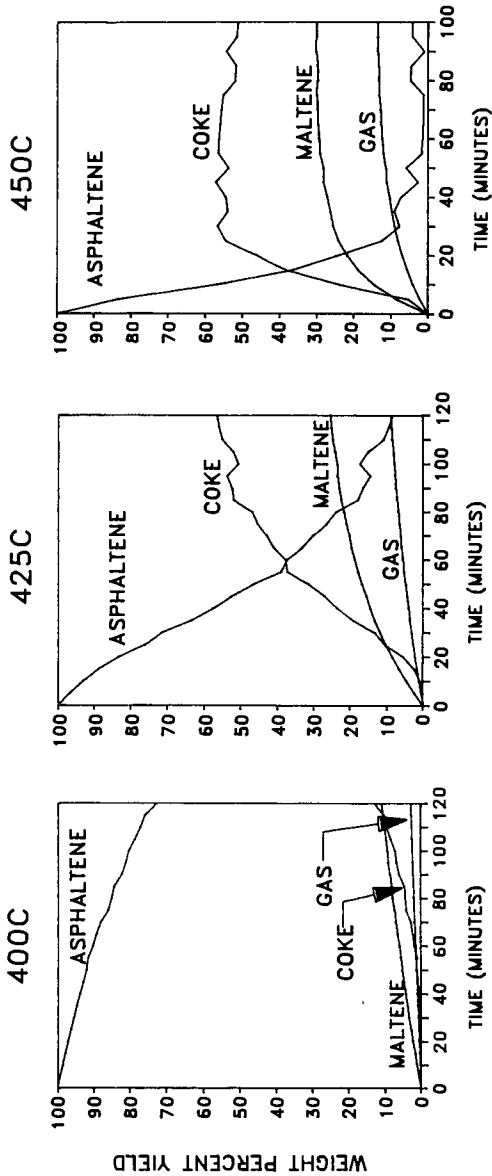
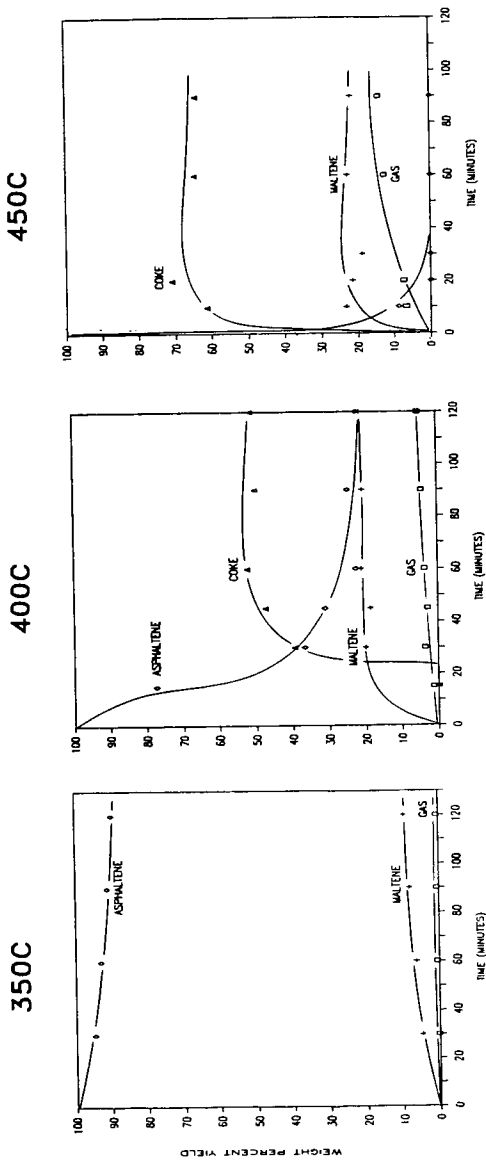


Figure 8: Temporal Variation of Product Fractions from Asphaltene Pyrolysis



INTERPRETING RAPID COAL DEVOLATILIZATION AS AN EQUILIBRIUM
FLASH DISTILLATION DRIVEN BY COMPETITIVE CHEMICAL KINETICS

Stephen Niksa

High Temperature Gasdynamics Laboratory
Mechanical Engineering Department
Stanford University
Stanford, CA 94305

Introduction

As the ambient pressure for a coal devolatilization process is reduced, ultimate yields of tar increase substantially. For high volatile bituminous coals, tar yields from vacuum pyrolysis can be fifty percent greater than from high-pressure pyrolysis. This behavior has long been attributed to competitive secondary chemistry in the gas phase occurring on a time scale dictated by transport of volatile matter through the particle surface. Among the escape mechanisms compatible with coal's complex physical structure, bulk and Knudsen pore diffusion, external film diffusion, continuum flow, and bubble growth in viscous melts have been treated, as reviewed recently by Suuberg (1).

These models correlate the reduced ultimate yield for increased ambient pressures, but important features of pyrolysis over a range of pressure remain unexplained. First, the measured rate of weight loss for identical thermal histories is the same for pressures between vacuum and 3.45 M Pa (2). Second, tar deposition exerts a negligible influence on both yields and evolution rates throughout all pressures of practical interest, based on the scaling from an independently-measured tar cracking rate and a measured volatiles escape rate (3). Third, the molecular weight distributions (MWD) of tar shift toward lower molecular weights as the ambient pressure is increased (1,4,5).

The reaction model introduced here (FLASHKIN) correlates the reduced ultimate yields, predicts evolution rates which are independent of pressure, and explains the observed shifts in tar MWD for varied ambient pressures. It interprets coal devolatilization as a single-stage equilibrium flash distillation driven by competitive chemical kinetics. While the mathematical formulation accommodates rate-limiting mass transport resistances, homogeneous chemistry is excluded and mass transport resistances are deemed negligible for the particle sizes considered in the comparisons with data. In this respect, FLASHKIN advances a minority viewpoint rooted in the parallels between pyrolysis and evaporative drying drawn by Peters and Bertling (6), and the aspects of phase equilibrium included in the models of James and Mills (7) and Niksa (8).

Reaction Mechanisms

The reaction mechanisms in FLASHKIN develop an analogy between coal pyrolysis and a single-stage equilibrium flash distillation. In any flash distillation, an equilibrium relation (such as Raoult's law in the simplest case) describes the partitioning of chemical species into the vapor and condensed phases at fixed pressure and temperature. The portion of the feedstream which evaporates is determined by a mole balance among the feed and product streams. Usually the composition and throughput of the feedstream and the temperature and pressure of the flash chamber are known, so that the composition and efflux of the vapor and liquid streams can be determined.

In the coal pyrolysis reaction system, there is no feedstream per se; rather, the coal macromolecule disintegrates into fragments which range in size from hydrocarbon gases having an average molecular weight of 25 g/mole to polymeric pieces of coal of molecular weight to, perhaps, 10^4 - 10^6 g/mole. The rate at which these species are introduced into the system is determined by the primary thermal reactions.

The flash chamber is, of course, the porous fuel particle. In softening coals, the vapor is fully dispersed throughout the melt as bubbles in a viscous liquid; otherwise, the vapor is dispersed throughout a pore system which delineates solid subunits of a few hundred angstroms in size (the size of mesopores). Regardless of the form of the condensed phase, we assume that their composition is uniform throughout the particle, because the characteristic dimension of the subunits of condensed matter is so small. The temperature of the system is externally imposed and, under the restriction of negligible internal heat transfer resistances, the particle is isothermal. But the internal pressure reflects the reaction dynamics. In actuality, the internal pressure reaches a level compatible with the generation rate of gases and the resistance to escape. Despite the modeling discussed earlier, the internal pressure remains ambiguous because coal's physical structure admits several plausible transport mechanisms, and also because the transport coefficients are uncertain. We assert that the time scale for mass transport is much shorter than the primary decomposition time, as applicable to continuum flow driven by a pressure gradient, and deduce that the internal and ambient pressures are nearly equivalent.

Since the primary decomposition fragments encompass light gases and high polymers, the vapor is regarded as a binary mixture of (a) noncondensibles, restricted to molecular weights below 100 to represent light gases, and (b) a continuous mixture of vapor fragments of molecular weight from 100 to infinity, to represent tar. The tar vapor is represented by a continuous MWD. The condensed phase is envisioned as a binary mixture of nonvolatile char and a continuous mixture of evaporating com-

pounds of molecular weight greater than 100; again, the condensed-phase continuous mixture is represented by a continuous MWD.

Equilibrium is asserted between the vapor and condensed continuous mixtures on the basis of scaling the molar concentrations in the vapor and condensed phases. Since the densities of gaseous and condensed species differ by three to four orders of magnitude, the accumulation of vapor within the particle is entirely negligible. In other words, the vapor composition is in quasi-steady equilibrium with the changing condensed phase composition. The time scale on which the phase equilibrium is established is the shortest in the system.

The compositions of the continuous mixtures in the vapor and condensed phases are related by a generalization of Raoult's law. This simple form is in keeping with the lack of data on high molecular weight coal products such as tar. Nevertheless, the formulation in FLASHKIN is more advanced than previous renderings of Raoult's law in pyrolysis modeling (7-9).

Until very recently, multi-component phase equilibrium was analyzed in terms of discrete pseudo-components presuming that basic thermodynamic relations expressed in terms of the mole fractions of the species apply, computational burdens notwithstanding. Their obvious limitation is that discrete mole fractions for mixtures as complex as coal tar are impossible to measure. "Continuous thermodynamics" circumvents this deficiency by recasting the conditions for phase equilibria in terms of continuous distributions of macroscopic characteristics such as aromaticity, carbon number, normal boiling point and, most pertinent to this model, molecular weight. Recent publications by Prausnitz and coworkers (10,11) and Ratzsch and Kehlen (12) develop the results used in FLASHKIN and access the literature on the general theory.

Finally, to complete the analogy between pyrolysis and a flash distillation, the efflux of vapor and liquid "products" must be specified. The efflux of vapor species is simply the sum of the evolution rates of gas and tar. Within the constraints of negligible mass transport restrictions and negligible vapor accumulation noted above, the escape rate of light gases must match the generation rate of gases from the primary thermal reactions; i. e., gases escape at their rate of production by chemical reaction. The tar evolution rate is also specified by this rate, with the additional constraints that mole fractions for the binary vapor sum to unity, and that phase equilibrium is maintained.

Of course, no condensed phase species leave the particle. But their efflux rate is analogous to the rate at which the condensed continuous mixture forms an involatile char. Lacking guidance from experiment, we assume that the char formation rate is independent of the molecular weight of the components in the mixture.

The basic structure of coal pyrolysis, especially tar evolution, shares many similarities with a single stage equilibrium flash distillation. The amount of tar in the vapor phase within the fuel particle is in equilibrium with a continuous mixture of high molecular weight fragments in either the solid subunits or viscous melt. Generation rates and the efflux of intermediates and products are established by chemical reaction rates. As elaborated in the full paper, the evolution rates of tar and light gases, and the tar MWD are completely specified by closing the mole balance among the reaction species.

References

1. Suuberg, E. M., in "Chemistry of Coal Conversion" (Ed. R. H. Schlosberg), Plenum Press, NY, 1985, pp. 67-120.
2. Niksa, S., Russel, W. B., and Saville, D. A., Nineteenth Symp. (Int.) on Comb., The Combustion Institute, Pittsburgh, 1982, p. 1151.
3. Niksa, S., Combust. Flame 66, 111 (1986).
4. Unger, P. E. and Suuberg, E. M., Fuel 63, 606 (1984).
5. Suuberg, E. M., Unger, P. E., and Lilly, W. D., Fuel 64, 966 (1985).
6. Peters, W. and Bertling, H., Fuel 44, 317 (1965).
7. James, R. K. and Mills, A. F., Lett. Heat Mass Transf. 5, 1 (1976).
8. Niksa, S. "Time Resolved Kinetics of Rapid Coal Devolatilization," Ph. D. Thesis, Department of Chemical Engineering, Princeton University, Princeton, NJ, 1982.
9. Unger, P. E. and Suuberg, E. M., Eighteenth Symp. (Int.) on Comb., The Combustion Institute, Pittsburgh, 1981, p. 1203.
10. Cotterman, R. L., Bender, R., and Prausnitz, J. M., Ind. Eng. Chem. Process Des. Dev. 24, 194 (1985).
11. Cotterman, R. L. and Prausnitz, J. M., Ind. Eng. Chem. Process Des. Dev. 24, 434 (1985).
12. Ratzsch, M. T. and Kehlen, H., Fluid Phase Equil. 14, 225 (1983).

A GENERAL MODEL OF COAL DEVOLATILIZATION

P.R. Solomon, D.G. Hamblen, R.M. Carangelo, M.A. Serio and G.V. Deshpande

Advanced Fuel Research, Inc., 87 Church St., East Hartford, CT 06108 USA

INTRODUCTION

Coal devolatilization is a process in which coal is transformed at elevated temperatures to produce gases, tar* and char. Gas formation can be related to the thermal decomposition of specific functional groups in the coal. Tar and char formation is more complicated. It is generally agreed that the tar formation includes the following steps which have been considered by a number of investigators.

1. The rupture of weaker bridges in the coal macromolecule to release smaller fragments called metaplasts (1).
2. Possible repolymerization (crosslinking) of metaplast molecules (2-14).
3. Transport of lighter molecules to the surface of the coal particles by diffusion in the pores of non-softening coals (5,8,15,16) and liquid phase or bubble transport in softening coals (17-19).
4. Transport of lighter molecules away from the surface of the coal particles by combined vaporization and diffusion (4,14).

Char is formed from the unreleased or recondensed fragments. Varying amounts of loosely bound "guest" molecules, usually associated with the extractable material, are also released in devolatilization.

The combined chemical and physical processes in devolatilization were recently reviewed by Gavalas (20) and Suuberg (21). While gas formation can be accurately simulated by models employing first order reactions with ultimate yields (3,22-29), success in mechanistic modeling of tar formation has been more limited. Predicting tar formation is important for many reasons. Tar is a major volatile product (up to 40% of the coal's weight for some bituminous coals). In combustion or gasification, tar is often the volatile product of highest initial yield and thus controls ignition and flame stability. It is a precursor to soot which is important to radiative heat transfer. The process of tar formation is linked to the char viscosity (9,17,30,31) and subsequent physical and chemical structure of the char and so is important to char swelling and reactivity. Also, because they are minimally disturbed coal molecule fragments, primary tars provide important clues to the structure of the parent coal (27,28,32).

This paper presents a general model for coal devolatilization which considers the evolution of gas, tar, char and guest molecules. The general model combines two previously developed models, a Functional Group (FG) model (25-29) and a Devolatilization-Vaporization-Crosslinking (DVC) model (12,13,33-36). The FG model considers the parallel independent evolution of the light gas species formed by the decomposition of functional groups. Alternatively, functional groups can be released from the coal molecule attached to molecular fragments which evolve as

*Tar is defined as the room temperature condensibles formed during coal devolatilization.

tar. The kinetic rates for the decomposition of each functional group and for tar formation have been determined by comparison to a wide variety of data (25-29). To a first approximation, these rates are insensitive to coal rank. The FG model uses an adjustable parameter to fit the total amount of tar evolution. This parameter depends strongly on the details of the time-temperature history of the sample, the external pressure, and the coal concentration and, therefore, varies with the type of experiment performed.

The variation in tar yield with the above mentioned parameters can be predicted by the DVC model (12,13,33-36). In the DVC model, tar formation is viewed as a combined depolymerization and surface evaporation process in which the pyrolytic depolymerization continually reduces the weight of the coal molecular fragments through bond breaking and stabilization of free radicals, until the fragments are small enough to evaporate and diffuse away from the surface. This process continues until the donatable hydrogens are consumed. Simultaneously, crosslinking can occur. The model employs a Monte Carlo technique to perform a computer simulation of the combined depolymerization, vaporization and crosslinking events. Until now, internal mass transport limitations have not been included. However, current research shows that considering the transport limitations of surface evaporation and film diffusion alone are not sufficient to predict the reduced tar yields when devolatilization occurs at low temperatures. An empirical expression for internal transport has, therefore, been added to the DVC model.

These two models have been combined to eliminate their respective deficiencies. The DVC model is employed to determine the yield of tar and molecular weight distribution in the tar and char. The FG model is used to describe the gas evolution, and the functional group compositions of the tar and char. The crosslinking is predicted by assuming that this event can be correlated with gas evolution.

The paper describes the two models and how they have been combined. The predictions of the FG-DVC model are compared to published data for product yields, extract yields, volumetric swelling ratio (determined by crosslink density) and molecular weight distributions for the devolatilizations of Pittsburgh Seam coal (2,3,9,12,28). The predictions are in good agreement with the data.

MODELS

General Description of Coal Devolatilization

The general outline of devolatilization employed in this work was recently presented by Solomon and Hamblen (27) and Serio et al. (28). Fig. 1 from Ref. 28 presents a hypothetical picture of the coal's or char's organic structure at successive stages of devolatilization. The figure represents: a) the raw coal, b) the formation of tar and light hydrocarbons during primary pyrolysis, and c) char condensation and crosslinking during secondary pyrolysis. The hypothetical structure in Fig. 1a represents the chemical and functional group compositions for a Pittsburgh Seam bituminous coal as discussed by Solomon (32). It consists of aromatic and hydroaromatic clusters linked by aliphatic bridges. During pyrolysis, the weakest bridges, labeled 1 and 2 in Fig. 1a, can break producing molecular fragments (depolymerization). The fragments abstract hydrogen from the hydroaromatics or aliphatics, thus increasing the aromatic hydrogen concentration. These fragments will be released as tar if they can get to a surface and vaporize, since they are small enough to vaporize under typical pyrolysis conditions, assuming the vaporization law proposed by Suuberg et al. (14) is correct. The

other two fragments are not small enough to vaporize.

The other events during primary pyrolysis are the decomposition of functional groups to release CO_2 , light aliphatic gases and some CH_4 and H_2O . The release of CH_4 , CO_2 , and H_2O may produce crosslinking, CH_4 by a substitution reaction in which the attachment of a larger molecule releases the methyl group, CO_2 by condensation after a radical is formed on the ring when the carboxyl is removed and H_2O by the condensation of two OH groups to produce an ether link (labeled 3 in Fig. 1b). The crosslinking is important to determine the release of tar and the visco-elastic properties of the char.

The end of primary pyrolysis occurs when the donatable hydrogen from hydroaromatics or aliphatics is depleted. During secondary pyrolysis (Fig. 1c) there is additional methane evolution (from methyl groups), HCN from ring nitrogen compounds, CO from ether links, and H_2 from ring condensation.

Functional Group Model

The Functional Group (FG) model developed in this laboratory has been described in a number of publications (25-29). It permits the detailed prediction of volatile species concentrations (gas yield, tar yield and tar functional group and elemental composition) and the chemical and functional group composition of the char. It employs coal independent rates for the decomposition of individual assumed functional groups in the coal and char to produce gas species. The ultimate yield of each gas species is related to the coal's functional group composition. Tar evolution is a parallel process which competes for all the functional groups in the coal. In the FG model, the ultimate tar yield is an input parameter which is adjusted for each type of experiment since the model does not include the mass transfer effects or char forming reactions which lead to tar yield variations.

FG Model Development - The FG model development was initiated by Solomon and Colket (25). A series of heated grid experiments were performed on a variety of coals in which individual products (gas species and tar) were monitored. It was noticed that while the ultimate yields of species varied from coal to coal and could be related to the coal's composition, the evolution rates for individual species were, to a good first approximation, independent of coal rank. Solomon and Hamblen examined a variety of literature data and found the insensitivity of individual species evolution rates to coal rank to be a general phenomenon (37). A similar conclusion was reached in a recent study by Xu and Tomita (38).

In subsequent work using entrained flow reactors (26-28) and a heated tube reactor (29), it was found that the general assumptions of the FG model were good, but that the original single activation energy rates derived from the heated grid experiments (25) were inaccurate. The use of a distributed activation energy rate expression, a wide variety of heating rates, and particle temperature measurements has provided more accurate and reactor independent kinetic rates for the present model (26-29). The general rates and specific composition parameters for Pittsburgh Seam coal are presented in Table I.

FG Model Formulation - The mathematical description of the functional group pyrolysis model has been presented previously (25-29). The evolution of tar and light gas species provides two competing mechanisms for removal of a functional group from the coal: evolution as a part of a tar molecule and evolution as a distinct gas species. Each process assumes a first order reaction,

$$dW_i(\text{gas})/dt = k_i W_i(\text{char}), \quad (1)$$

where, $dW_i(\text{gas})/dt$ is the rate of evolution of species i into the gas phase, k_i is its rate constant and $W_i(\text{char})$ is the functional group source remaining in the char. Note that $W_i(\text{char})$ also is decreased by evolution of the source with the tar, according to,

$$dW_i(\text{tar})/dt = k_{\text{tar}} W_i(\text{char}). \quad (2)$$

The reduction of $W_i(\text{char})$ is thus,

$$-dW_i(\text{char})/dt = dW_i(\text{gas})/dt + dW_i(\text{tar})/dt \quad (3)$$

The kinetic rates, k_i and k_{tar} , for each functional group employs a distributed activation energy of the form used by Anthony et al. (2).

The Depolymerization-Vaporization-Crosslinking (DVC) Model

The Depolymerization-Vaporization-Crosslinking model has been described in a number of publications (12,13,33-36). It predicts the tar yield, the tar molecular weight distribution, the char yield, the char molecular weight distribution, the extract yield and the crosslink density.

DVC Model Development - The model had its beginning in a study of polymers representative of structural features found in coal (33). The objective of that study was to develop an understanding of coal pyrolysis by studying a simpler, more easily interpretable system. The polymers were studied in a series of pyrolysis experiments in which tar amounts and molecular weights were measured. A theory was developed to describe the combined effects of: i) random bond cleavage in long polymer chains (similar to Gavalas et al. (39)), ii) molecular weight dependent vaporization of the fragments to produce tar (similar to Unger and Suuberg (4)), and iii) a limitation on the number of breakable bonds which depended on the availability of donatable hydrogens to cap the free radicals formed by the cleavage.

The model was subsequently improved by Squire et al. (35,36) by adding the chemistry for the consumption of donatable hydrogens to cap free radicals along with corresponding carbon-carbon double bond formation at the donor site. In the polymers which were studied, the ethylene bridges were identified as a source of donatable hydrogen with the formation of a double bond between the bridge carbons (35,36). The double bond formation was assumed to remove a breakable bond. This improvement in the model removed the donatable hydrogen as an adjustable parameter. It should be noted that hydroaromatic groups are also a source of donatable hydrogen with aromatization of the ring, however, for simplicity, the DVC model assumes all donatable hydrogens are in bridges. The model was further improved by the implementation of a Monte Carlo method for performing the statistical analysis of the bond breaking, the hydrogen consumption and the vaporization processes. A single kinetic rate described the random bond breaking. This kinetic rate (35) employs an activation energy which is in agreement with resonance stabilization calculations (40,41) and an overall rate which agrees with previous measurements on model compounds (42). The rate determined for the breaking of ethylene bridges between naphthalene rings is in good agreement with the rate for tar formation from coal (28,29). The model predicted the observed molecular weight distribution and dependence of yield with the availability of donatable hydrogen. The results for model polymers compared favorably with many of the details of tar formation in softening coals. However, in the version of the model reported in Ref. 35, there

was no explicit char forming reaction. Char consisted of molecular fragments which were too heavy to vaporize and thus remained after the donatable hydrogen had been consumed.

Crosslinking Reactions - The next improvement in the model to be reported (12,13,35) was the addition of char forming repolymerization (crosslinking) reactions. These reactions are important in describing the rank and heating rate dependence of the tar molecular weight distributions and yields. Work has been performed to define the reactions which cause crosslinking (43-45). Under the assumption that the crosslinking reactions may also release gas species, the molecular weight between crosslinks or crosslink density (estimated using the volumetric swelling technique developed by Larsen and co-workers (46-48)) was correlated with the observed evolution of certain gas species during pyrolysis. Likely candidates were CO₂ formation from carboxyl groups or methane formation from methyl groups. Suuberg et al. (48) also noted that crosslinking in low rank coals is correlated with CO₂ evolution. Both reactions may leave behind free radicals which can be stabilized by crosslinking. Condensation of hydroxyl groups to form water and an ether link is also a possible reaction.

For a series of chars, the loss of volumetric swelling ratio in pyridine was compared with CO₂ evolution for a Zap, North Dakota lignite and CH₄ evolution for a Pittsburgh Seam bituminous coal (44). The lignite reaches maximum crosslinking before the start of methane evolution and the Pittsburgh Seam bituminous evolves little CO₂. On a molar basis, the evolution of CO₂ from the lignite and CH₄ from the bituminous coal appear to have similar effects on the volumetric swelling ratio. The results suggest that one crosslink is formed for each CO₂ or CH₄ molecule evolved. No correlation was observed between the volumetric swelling ratio and tar yield for either coal. A correlation with water yield appears valid for the Zap, North Dakota lignite, but not for the Pittsburgh Seam bituminous coal.

DVC Model Description - In the current DVC model, the parent coal is represented as a two-dimensional network of monomers linked by strong and weak bridges as shown in Fig. 2a. It consists of condensed ring clusters (monomers) linked to form an oligomer of length "n" by breakable and non-breakable bridges. The clusters are represented by circles with molecular weights shown in each circle. The breakable bridges (assumed to be ethylene) are represented by single lines, the unbreakable bridges by double lines. "m" crosslinks are added so that the molecular weight between crosslinks corresponds to the value reported in the literature (49) for coals of similar rank. Unconnected "guest" molecules (the extract yield) are obtained by choosing the value of n. The ratio of ethylene bridges (two donatable hydrogens per bridge) to non-breakable bridges (no donatable hydrogens) is chosen to obtain the appropriate value for total donatable hydrogen. The parameters for a Pittsburgh Seam coal are presented in Table II.

Figure 2b shows the molecule during pyrolysis. Some bonds have broken, other bonds have been converted to unbreakable bonds by the abstraction of hydrogen to stabilize the free radicals and new crosslinks have been formed. Char formation in the DVC model can occur by crosslinking at any monomer to produce a two dimensional crosslinked network.

Figure 2c shows the final char which is highly crosslinked with unbreakable bonds and has no remaining donatable hydrogen.

The Combined FG-DVC Model

A detailed description of the pyrolysis behavior of coal is obtained by

combining the DVC model with the FG model. The FG model predicts the gas yields, and using the correlation developed for crosslinking with gas yields, it also determines the rate and number of crosslinks formed, assuming one crosslink is formed per CO₂ or CH₄ molecule evolved, for the DVC model. The DVC model supplies the tar yield to the FG model, replacing what was previously an adjustable parameter. It also supplies the number of new methyl groups formed and the concentration of C₂H₄ and C₂H₂ bridges.

FG-DVC Model Description - The model is initiated by specifying the Functional Group composition and the parameters (number of breakable bridges, starting oligomer length n, number of added crosslinkings, m, and the monomer molecular weight distribution). The starting DVC molecule is represented in Fig. 2a. The monomers are assumed to have the average elemental and functional group composition given by the FG model. Each computer simulation considers a coal molecule consisting of 2400 monomers. The model has been programmed in Fortran 77 and run on an Apollo DN580 computer.

Once the starting coal molecule is established, it is then subjected to a time-temperature history made up of a series of isothermal time steps. During each step, the gas yields, elemental composition and functional group compositions are computed using the FG model. To determine the change of state of the computer molecule during a time step, the number of crosslinks formed is determined using the FG model, and then input to the DVC model. These crosslinks are distributed randomly throughout the char, assuming that crosslinking probability is proportional to the molecular weight of the monomer. Then the DVC model breaks the appropriate number of bridging bonds (assuming a distribution of activation energies for the bond breaking rates) and calculates the quantity of tar evolved for this time step using the vaporization law. The modified expression of Suuberg et al. (14) is now employed for the vaporization law rather than that of Unger and Suuberg (4). A fraction of the abstractable hydrogen is used to stabilize the free radicals formed by bridge breaking and the appropriate fraction of breakable bridges is converted into (unbreakable) double-bonds. Tar formation is complete when all the donatable hydrogen is consumed. A typical simulation for a complete time temperature history takes about ten minutes.

Internal Transport Limitations - When comparing the predictions of the model to available data it was found that tar yields were overpredicted when devolatilization occurred at low temperatures. This was observed for either low heating rate experiments (28) or experiments with rapid heating to relatively low temperatures (9). As discussed in the Results Section, it appears that the lower yields were the result of the additional transport limitations within the particle. This limitation can be: i) the transit of bubbles containing tar from the interior of the particle to the surface; ii) the transport of tars within the liquid to the bubble; iii) the stirring action of the bubble. In the absence of sufficient information to accurately model these processes, the simple assumption was made that tars are carried out of the particle at their equilibrium vapor pressure in the light devolatilization products.

Then,

$$(dn_i/dt)_{tr} = P_{si} X_i \sum_{\substack{\text{light} \\ \text{products}}} (dn_i/dt)_{chem} \frac{1}{P_o + \Delta P} \quad (4)$$

where $(dn_i/dt)_{tr}$ is the transport rate for tar component i, of number in the particle n_i . $(dn_i/dt)_{chem}$ is the rate of production of component i. P_o is the

ambient pressure, P_{gi} is the equilibrium vapor pressure for component i (given by Suuberg et al. (14)) and ΔP is the average pressure difference in the particle which drives the transport. X_i is the mole fraction of component i in the metaplast. For the highly fluid Pittsburgh Seam bituminous coal, we have considered the upper limit to this rate where $P_0 \gg \Delta P$. Then all the terms in Eq. 1 can be determined by the combined FG-DVC model.

The net rate for tar transport is calculated by assuming that the resistance to internal and external transport occur in series. For melting coals ΔP is proportional to the coal's viscosity and so, will become important for less fluid coals. It is also important when P_0 is small.

Summary of FG-DVC Model Assumption - Assumptions a-c are made for the FG model and d-n for the DVC model.

(a) Light gas species are formed from the decomposition of specific functional groups with rate coefficients which depend on the functional group but are insensitive to coal rank. The evolution rate is first order in the remaining functional group concentrations in the char. The rates follow an Arrhenius expression with a Gaussian distribution of activation energies (2,26,27).

(b) Simultaneous with the production of light gas species, is the thermal cleavage of bridge structures in the coal to release molecular fragments of the coal (tar) which consist of a representative sampling of the functional group ensemble. The instantaneous tar yield is given by the DVC model.

(c) Under conditions where pyrolysis products remain hot (such as an entrained flow reactor), pyrolysis of the functional groups in the tar continues at the same rates used for functional groups in the char, (e.g., the rate for methane formation from methyl groups in tar is the same as from methyl groups in the char).

(d) The oligomer length, n , the number of crosslinks, m , and the number of unbreakable bonds are chosen to be consistent with the coal's measured extract yield, crosslink density and donatable hydrogen concentration.

(e) The molecular weight distribution is adjusted to best fit the observed molecular weight distribution for that coal, measured by pyrolysis of the coal (in vacuum at 3°C/min to 450°C) in a FIMS apparatus (50). Molecular weights 106, 156, 206, 256, 306, 356 and 406 (which are 1,2,3,4,5,6 and 7 aromatic ring compounds with two methyl substituents) are considered as representative of typical monomer molecular weights.

(f) During pyrolysis, the breakable bonds are assumed to rupture randomly at a rate k , described by an Arrhenius expression with a Gaussian distribution of activation energies. Each rupture creates two free radicals which consume two donatable hydrogens to stabilize and form two new methyl groups.

(g) Two donatable hydrogens (to cap free radicals) are available at each breakable bridge. The consumption of the donatable hydrogen converts the bridge into an unbreakable bridge by the formation of a double bond.

(h) Tar formation continues until all the donatable hydrogens are consumed.

(i) During pyrolysis, additional unbreakable crosslinks are added at a rate determined by the evolution of CH_4 and CO_2 . One crosslink is created for each evolved molecule. The rate of CH_4 and CO_2 evolution is given by the FG model.

(j) The crosslinks are distributed randomly, with the probability of attachment on any one monomer being proportional to the molecular weight of the monomer.

(k) Tar molecules are assumed to evaporate from the surface of the coal particle at a molecular weight dependent rate controlled by evaporation and gas phase diffusion away from the particle surface. The expressions derived by Suuberg et al. (14) are employed.

(l) Internal transport resistance is assumed to add to the surface transport resistance. A simple empirical expression (Eq. 4) was used to describe bubble transport resistance in softening coals. This appears to be the step most in need of further work.

(m) Extractable material (in boiling pyridine) in the char is assumed to consist of all molecules less than 3000 AMU. This can be adjusted depending on the solvent and extract conditions.

(n) The molecular weight between crosslinks, M_c is computed to be the total molecular weight in the computer molecule divided by the total number of crosslinks. This assumption will underestimate M_c since broken bridges are not considered.

RESULTS

The model predictions have been compared to the results obtained from a number of experiments on the pyrolysis of a Pittsburgh Seam coal at AFR and MIT (2,3,9,28). The coal composition parameters are presented in Tables I and II. It should be noted that different samples of Pittsburgh seam coal from different sources were employed. While the elemental compositions were similar, extract yields varied substantially depending on the sample source. The oligomer length was chosen to fit an extract yield of 30%. It is expected that yields may vary slightly from predictions for other samples, but the predicted rates should be sample independent. Comparisons are considered for gas yields, tar yields, tar molecular weight distributions, extract yields and volumetric swelling ratio.

Volatile and Extract Yields

Extensive comparisons of the FG model with gas yields have been presented previously (27-29) and won't be repeated here. The Functional Group parameters and the kinetic rates for the Pittsburgh Seam coal are those published in Ref. 28. The methane parameters for the Pittsburgh Seam coal were adjusted (methane X-L = 0.0, methane-L = 0.02, methane-T = 0.015, unchanged) to better match yield of Refs. 2, 27 and 28 (see Fig. 20c in Ref. 28). A second modification is that the CH_x -aliphatic rate in Ref. 28 applies to the observed gas species (paraffins, olefins, C_2H_6 , C_2H_4) only. The aliphatic material in the CH_x -aliphatic group is assumed to be made up of bridges which volatilize only when attached to a tar molecule (i.e., $k_{bridge} = 0$). Results for methane are considered because the methane is associated with crosslinking. The CO_2 yields are not considered in this paper since they are too low in the Pittsburgh Seam coal to cause significant crosslinking.

Figure 3 compares the FG-DVC predictions to the data of Fong et al. (9) on total volatile yield and extract yield as a function of temperature in pyrolysis at 0.85 ATM. The experiments were performed in a heated grid at heating rates of approximately 500°C/sec, variable holding times and rapid cool down. The predictions at the two higher temperatures (3c and 3d) are in excellent agreement

with the data. Having fixed all the rates and functional group compositions based on previous work, the only adjustable parameters were the number of labile bridges (which fixes the donatable hydrogen concentration) and the monomer distribution, assumed to be Gaussian. The predictions for the two lower temperatures were not good when internal transport limitations were neglected. The dashed line in Fig. 3a shows the predicted yield in the absence of internal transport limitations. The predicted ultimate yield is clearly too high. The data suggest that the low yields are not a result of unbroken bonds (which would result from a lower bond breaking rate), since the extract yields at low temperatures are equivalent to those at the higher temperatures. The low yields thus appear to be a result of an additional transport limitation.

Equation 4 was employed for the internal transport resistance and the number of labile bridges were readjusted for the 1018°K case. The predictions are the solid lines in Fig. 3. The internal transport limitation is important when pyrolysis occurs at low temperatures and $\frac{dn_i}{dt}$ is small. It is much less important for the 1018K and 992K cases, making only a small difference in the predicted yields.

There still is a discrepancy between the prediction and the data at early times for the two lower temperatures (Figs. 3a and b). While it is possible that the rate k for bond breaking is too high, adjustment of this rate alone significantly lowers the extractable yield, since the lower depolymerization rate is closer to the methane crosslinking rate. In addition, both the methane and depolymerization rates appear to be in good agreement with the data at even lower temperatures, as shown in Fig. 4 (discussed below). Another possibility is that the coal particles heat more slowly than the nominal temperatures given by Fong et al. (9). Such an effect could be caused by having some clumps of particle which would heat more slowly than isolated particles, by reduction in the convective heat transfer due to the volatile evolution (blowing effect), or by endothermic tar forming reactions. A firm conclusion as to the source of the discrepancy cannot be drawn without further investigation.

It is also seen in Figs. 3a and b that the crosslinking rate is higher than predicted. This can be due to additional methane from methyl groups created during tar formation, which is not yet counted in the model, or to other crosslinking events not considered. These possibilities are currently under investigation.

Figure 4 presents comparisons of devolatilization yields at slow (30°C/min), heating rates in a thermogravimetric analyzer with Fourier transform infrared analysis of evolved products (TG-FTIR). This reactor has been previously described (51). The model predictions and experimental results are in excellent agreement. The agreement validates the assumed rates for depolymerization and crosslinking produced by CH_4 at low temperatures. Also, the use of Eq. 4 appears to predict the appropriate drop in tar yield (maximum value 17%) compared to 30% when devolatilization occurs at high temperature.

Pressure Effects

The predicted effect of pressure on the tar molecular weight distribution is illustrated in Figs. 5a and b. The average molecular weight and the vaporization "cut-off" decrease with increasing pressure. The trends are in agreement with observed tar molecular weight distributions shown in Figs. 5c and d. The spectra are for previously formed tar which has been collected and analyzed in a FIMS apparatus (50). The low values of intensity between 100 and 200 mass units is due

to loss of these components in collection and handling due to their high volatility.

Pressure effects on yields have been examined. Figure 6 compares the predicted and measured pressure dependence on yield. Figure 6a compares to the total volatile yield data of Anthony et al. (2) while Fig. 6b compares to the tar plus liquids data of Suuberg et al. (3). The agreement between theory and experiment is good at one atmosphere and above, but overpredicts the yields at low pressure. Below one atmosphere, it is expected that ΔP within the particle will become important compared to the ambient pressure, P_0 .

CONCLUSIONS

A general model for coal devolatilization which combines a functional group model for gas evolution and a statistical model for tar formation has been presented. The tar formation model includes depolymerization, vaporization, crosslinking and internal transport resistance. The crosslinking is related to the formations of CO_2 and CH_4 species evolution, with one crosslink formed per molecule evolved. The predictions of the tar formation model are made using Monte Carlo methods.

The general model predictions compare favorably with a variety of data for the devolatilization of Pittsburgh Seam coal, including volatile yields, extract yields, and tar molecular weight distributions. The variations with pressure and devolatilization temperature were accurately predicted. While film diffusion appears to limit surface evaporation and the transport of tar when devolatilization occurs at high temperatures, internal transport appears to become dominate when devolatilization occurs at low temperatures.

ACKNOWLEDGMENT

This work was supported under DOE Contracts DEAC21-85MC22050, DEAC21-84MC21004 and DE-AC21-86MC23075. The authors wish to express their thanks to Professor Eric Suuberg for many helpful discussions on transport properties.

REFERENCES

1. van Krevelen, D.W. and Schuyer, J., *Coal Science*, Elsevier, Amsterdam, (1957).
2. Anthony, D.B., Howard, J.B., Hottel, H.C., and Meissner, H.P., 15th Symp. (Int) on Combustion, The Combustion Institute, Pittsburgh, PA, pg. 1303, (1974).
3. Suuberg, E.M., Peters, W.A., and Howard, J.B., 17th Symp. (Int) on Combustion, The Combustion Institute, Pittsburgh, PA, pg. 117, (1979).
4. Unger, P.E. and Suuberg, E.M., 18th Symp. (Int) on Combustion, The Combustion Institute, Pittsburgh, PA, pg. 1203, (1981).
5. Russel, W.B., Saville, D.A., and Greene, M.I., *AIChE J.*, **25**, 65, (1979).
6. James, R.K. and Mills, A.F., *Letters in Heat and Mass Transfer*, **3**, 1, (1976).
7. Lewellen, P.C., S.M. Thesis, Department of Chemical Engineering, MIT, (1975).
8. Chen, L.W. and Wen, C.Y., *ACS Div. of Fuel Chem. Preprints*, **24**, (3), p141, (1979).
9. Fong, W.S., Peters, W.A., and Howard, J.B., *Fuel*, **65**, 251, (1986).
10. Niksa, S. and Kerstein, A.R., *Combustion and Flame*, **66**, #2, 95, (1986).
11. Niksa, S. *Combustion and Flame*, **66**, #2, 111, (1986).
12. Solomon, P.R., Squire, K.R., Carangelo, R.M., proceedings of the International Conference on Coal Science, Sydney, Australia, pg. 945, (1985).
13. Solomon, P.R. and Squire, K.R., *ACS Div. of Fuel Chem. Preprints*, **30**, #4, 347,

- (1985).
14. Suuberg, E.M., Unger, P.E., and Lilly, W.D., *Fuel*, **64**, 956, (1985).
 15. Gavalas, G.R. and Wilks, K.A., *AIChE*, **26**, 201, (1980).
 16. Simons, G.A., *Prog. Energy Combust. Sci.*, **9**, 269, (1983).
 17. Oh, M., Peters, W.A., and Howard, J.B., *Proc. of the 1983 Int. Conf. on Coal Sci.*, p 483, International Energy Agency, (1983).
 18. Suuberg, E.M. and Sezen, Y., *Proc. of the 1985 Int. Conf. on Coal Sci.*, p913, Pergamon Press, (1985).
 19. Melia, P.F. and Bowman, C.T., *Combust. Sci. Technol.* **31**, 195 (1983); also An analytical model for coal particle pyrolysis and swelling, paper presented at the Western States Section of the Combustion Institute, Salt Lake City, 1982.
 20. Gavalas, G.R., *Coal Pyrolysis*, Elsevier (1982).
 21. Suuberg, E.M., in *Chemistry of Coal Conversion*, (R.H. Schlosberg, Ed.), Chapter 4, Plenum Press, NY (1985).
 22. Juntgen, H. and van Heek, K.H., *Fuel Processing Technology*, **2**, 261, (1979).
 23. Weimer, R.F. and Ngan, D.Y., *ACS Div. of Fuel Chem. Preprints*, **24**, #3, 129, (1979).
 24. Campbell, J.H., *Fuel*, **57**, 217, (1978).
 25. Solomon, P.R. and Colket, M.B., 17th Symposium (Int) on Combustion, The Combustion Institute, Pittsburgh, PA, 131, (1979).
 26. Solomon, P.R., Hamblen, D.G., Carangelo, R.M., and Krsuse, J.L., 19th Symposium (Int) on Combustion, The Combustion Institute, Pittsburgh, PA, 1139, (1982).
 27. Solomon, P.R. and Hamblen, D.G., in *Chemistry of Coal Conversion*, (R.H. Schlosberg, Editor), Plenum Press, NY, Chapter 5, pg. 121, (1985).
 28. Serio, M.A., Hamblen, D.G., Markham, J.R., and Solomon, P.R., *Energy and Fuels*, **1**, (2), 138, (1987).
 29. Solomon, P.R., Serio, M.A., Carangelo, R.M., and Markham, J.R., *Fuel*, **65**, 182, (1986).
 30. Fong, W.S., Khalil, Y.F., Peters, W.A. and Howard, J.B., *Fuel*, **65**, 195 (1986).
 31. van Krevelen, D.W., *Properties of Polymers*, Elsevier, Amsterdam (1976).
 32. Solomon, P.R., *New Approaches in Coal Chemistry*, ACS Symposium Series 169, American Chemical Society, Washington, DC, pp 61-71, (1981).
 33. Solomon, P.R. and King, H.H., *Fuel*, **63**, 1302, (1984).
 34. Solomon, P.R., Squire, K.R., and Carangelo, R.M., *ACS Div. of Fuel Chem. Preprints*, **29**, #2, 84, (1984).
 35. Squire, K.R., Solomon, P.R., DiTaranto, M.B., and Carangelo, R.M., *Fuel*, **65**, 833, (1986).
 36. Squire, K.R., Solomon, P.R., DiTaranto, M.B., and Carangelo, R.M., *ACS Div. of Fuel Chem. Preprints*, **30**, #1, 386, (1985).
 37. Solomon, P.R. and Hamblen, D.G., *Prog. Energy Comb. Sci.*, **9**, 323, (1983).
 38. Xu, W.-C., and Tomita, A., *Fuel*, **66**, 632 (1987).
 39. Gavalas, G.R., Cheong, P.H., and Jain, R., *Ind. Eng. Chem. Fundam.* **20**, 113, and 122, (1981).
 40. Stein, S.E., *New Approaches in Coal Chemistry*, (B.D. Blaustein, B.C. Bockrath, and S. Friedman, Editors), ACS Symposium Series, 169, 208, Am. Chem. Soc. Washington, DC, (1981).
 41. Stein, S.E., "Multistep Bond Breaking and Making Processes of Relevance to Thermal Coal Chemistry", Annual Report for GRI Contract No. 5081-261-0556. Accession No. GRI-81/0147, (1983).
 42. Stein, S.E., Robaugh, D.A., Alfieri, A.D., and Miller, R.E., "Bond Homolysis in High Temperature Fluids", *Journal of Amer. Chem. Society*, **104**, 6567, (1982).
 43. Solomon, P.R., Serio, M.A., and Deshpande, G.V., "Crosslinking Reactions in Coal Liquefaction", presented at the DOE Contractor's Review Conference, Monroeville, PA, (1986).

44. Solomon, P.R., Hamblen, D.G., Carangelo, R.M., Serio, M.A., and Deshpande, G.V., "Models of Tar Formation During Coal Devolatilization", submitted to *Combustion and Flame*, (1987).
45. Solomon, P.R., Hamblen, D.G., Deshpande, G.V. and Serio, M.A., A General Model of Coal Devolatilization, International Coal Science Conference, The Netherlands, October 1987.
46. Green, T.K., Kovac, J., and Larsen, J.W., *Fuel*, **63**, #7, 935, (1984).
47. Green, T.K., Kovac, J., and Larsen, J.W., in Coal Structure, (R.A. Meyers, Editor), Academic Press, NY, (1982).
48. Suuberg, E.M., Lee, D., and Larsen, J.W., *Fuel*, **64**, 1668, (1985).
49. Nelson, J.R., *Fuel*, **62**, 112, (1983).
50. St. John, G.A., Bustrill, Jr., S.E. and Anbar, M., ACS Symposium Series, **71**, p. 223 (1978).
51. Carangelo, R.M. and Solomon, P.R., *Fuel*, **66**, (1987), accepted for publication.

Table I. Kinetic Rate Coefficients and Species Compositions for Pittsburgh Seam Coal

composition parameters	gas	primary functional group source	rate equation ^a	Pittsburgh No. 8 bituminous coal
C				0.821
H				0.056
N				0.017
S(organic)				0.024
O				0.082
total				1.000
Y ₁	CO ₂ extra loose	carboxyl	k ₁ = 0.56E+18 exp(-30000±2000/T)	0.000
Y ₂	CO ₂ loose	carboxyl	k ₂ = 0.85E+17 exp(-33850±1500/T)	0.006
Y ₃	CO ₂ tight		k ₃ = 0.11E+18 exp(-38316±2000/T)	0.005
Y ₄	H ₂ O loose	hydroxyl	k ₄ = 0.22E+19 exp(-30000±1500/T)	0.011
Y ₅	H ₂ O tight	hydroxyl	k ₅ = 0.17E+14 exp(-32700±1500/T)	0.011
Y ₆	CO ether loose		k ₆ = 0.14E+19 exp(-40000±6000/T)	0.050
Y ₇	CO ether tight	ether O	k ₇ = 0.16E+16 exp(-40600±1600/T)	0.022
Y ₈	HCN loose		k ₈ = 0.17E+14 exp(-30000±1500/T)	0.009
Y ₉	HCN tight		k ₉ = 0.69E+13 exp(-42500±4750/T)	0.022
Y ₁₀	NH ₃		k ₁₀ = 0.12E+13 exp(-27300±3000/T)	0.000
Y ₁₁	CH ₄ aliphatic	H(al)	k ₁₁ = 0.84E+15 exp(-30000±1500/T)	0.190
Y ₁₂	methane extra loose	methoxy	k ₁₂ = 0.84E+15 exp(-30000±1500/T)	0.000
Y ₁₃	methane loose	methyl	k ₁₃ = 0.75E+14 exp(-30000±2000/T)	0.020
Y ₁₄	methane tight	methyl	k ₁₄ = 0.34E+12 exp(-30000±2000/T)	0.015
Y ₁₅	H aromatic	H(ar)	k ₁₅ = 0.10E+15 exp(-40500±6000/T)	0.012
Y ₁₆	methanol		k ₁₆ = 0.00E+00 exp(-30000±0/T)	0.000
Y ₁₇	CO extra tight	ether O	k ₁₇ = 0.20E+14 exp(-45500±1500/T)	0.020
Y ₁₈	C nonvolatile	C(ar)	k ₁₈ = 0	0.583
Y ₁₉	S organic			0.024
total				1.000
X ₁	tar		k _T = 0.96E+15 exp(-27700±1500/T)	

^a The Rate Equation is of the Form $k_n = k_0 \exp(-E/RnT)$, with k_0 in $\text{m}^3/\text{m}^2 \cdot \text{h}$, E in K, and R in K.

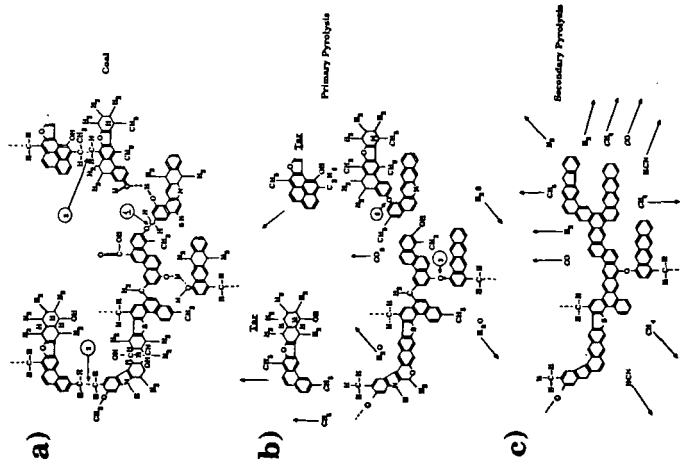


Figure 1. Hypothetical Coal Molecule During Stages of Pyrolysis. (reprinted from Ref. 28).

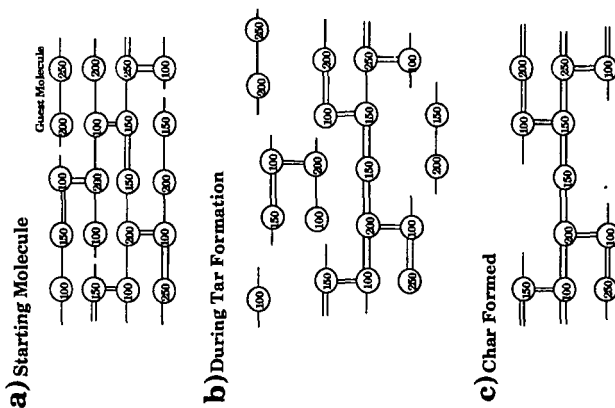


Figure 2. Representation of Coal Molecule in the DVC Simulation. The Circles Represent the Monomers (ring clusters and peripheral groups). The Molecular Weight Shown by the Numbers is the Molecular Weight of the Monomer Including the Attached Bridges. The Single Line Bridges are Breakable and can Donate Hydrogen. The Double Line Bridges are Unbreakable and do not Donate Hydrogen.

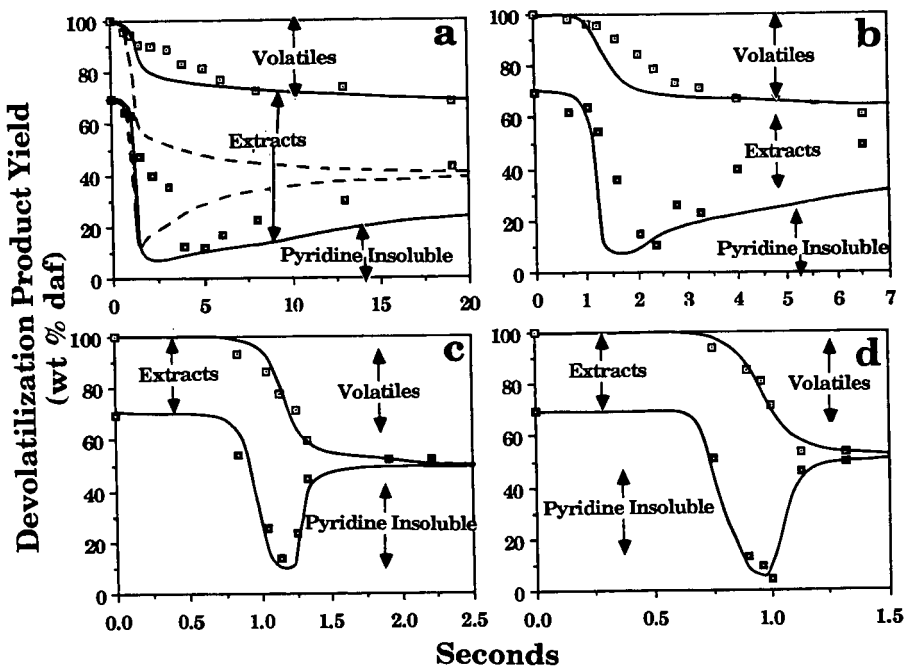


Figure 3. Comparison of FG-DVC Model Predictions (lines) with the Data of Fong et al (9) (symbols) for Pittsburgh Seam Coal. a) 813K @ 470 k/s, b) 858K @ 446k/s, c) 992K @ 514k/s and d) 1018K @ 640k/s. P=0.85 atm. The Dashed Line in a Shows the Predicted Yield in the Absence of Internal Transport Limitations.

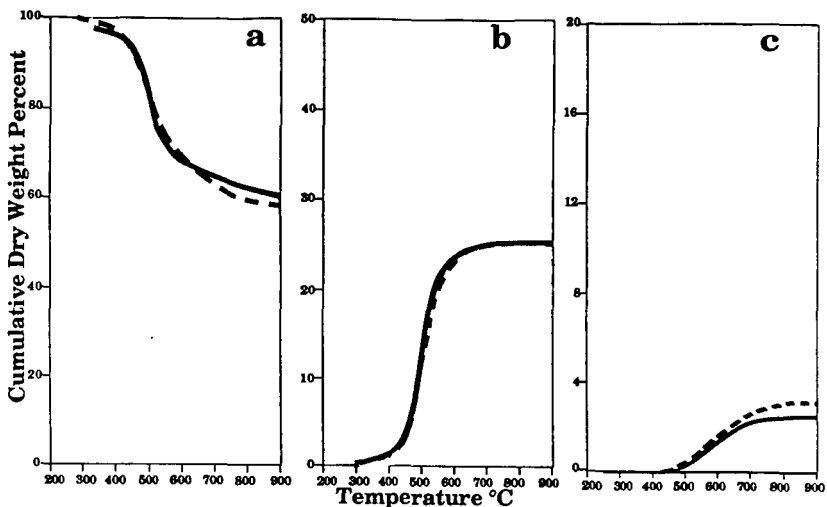


Figure 4. Comparison of Measured (solid line) and Predicted (dashed line) Volatile Yields for Pittsburgh Seam Coal Heated in Helium in a TG-FTIR at 0.5°C/sec to 900°C. a) Weight Loss, b) Tar Plus Aliphatics, and c) Methane.

TABLE II
PARAMETERS FOR DVC MODEL

		PITTSBURGH BITUMINOUS
Labile bridges	W_1 (wt.%)	9.6
Nuclei (ring clusters)	W_2^* from FG model (wt.%)	56.2
Peripheral groups	W_3 from FG model (wt.%)	34.2
Donatable hydrogens	$(2/28)W_1$	0.68
No. of crosslinks in coal	m #/monomer	0.095
Oligomer length	n #/oligomer	8
No. of potential crosslink sites (CO ₂)	a #/monomer	0.07
No. of potential crosslink sites (CH ₄)	b #/monomer	0.42

MOLECULAR WEIGHTS

Labile bridges	Fixed at 28	28
Monomers	Distribution ⁺ M_{avg} , (\bar{G})	256, (250)
Gas	From FG model	
Tar	Predicted in model from vaporization law	
Non-labile bridges	Fixed at 26	26

* Carbon in aromatic rings plus non-labile bridges

+ Gaussian Distribution

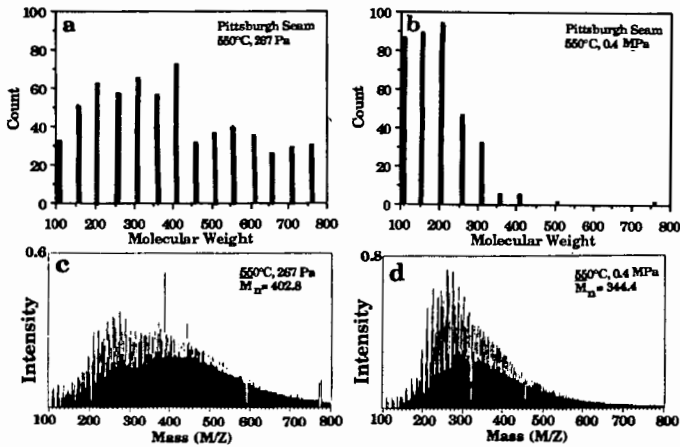


Figure 5. Comparison of Predicted (a and b) and Measured (c and d) Tar Molecular Weight Distribution for Pyrolysis of a Pittsburgh Seam Coal in a Heated Grid Apparatus at a Heating Rate of 500°C/sec to 550°C. Figure a and c Compare the Prediction and the Measurement at 267 Pa. Figure b and d Compare the Prediction and Measurement at 0.4 MPa.

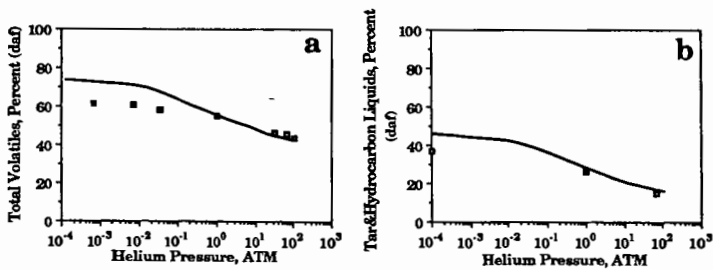


Figure 6. Comparison of Measurement and Prediction of Product Yields as a Function of Pressure. a) Volatile vs. Pressure (data from Anthony et al.(2)) and b) Tar Plus Liquids vs. Pressure Data from Suuberg et al. (3).

KINETIC MODELING OF COAL PYROLYSIS IN A LAMINAR-FLOW REACTOR SYSTEM

William S. O'Brien, Juh Wah Chen, Asadollah Moslehi and Rong-Chen Richard Wu

Mechanical Engineering and Energy Processes Department
Southern Illinois University at Carbondale
Carbondale, Illinois 62901-6603

INTRODUCTION

There will soon be an intense competition in the energy marketplace among oil, natural gas, coal, nuclear fission and the newly developing alternatives of solar, wind and waste utilization. The charge to the energy-entrepreneurs is to intensify their search to recognize and exploit the most economical and technically expedient manner of converting these raw energy sources into acceptable forms for the public's use.

Coal will certainly play a leading role in supplying the future energy needs of this nation's industrial and commercial ventures. But coal is an extremely complex heterogeneous material, composed of a number of distinct organic entities, called macerals, and inorganic minerals. Coals from different coal seams and even from separated points in the same seam often behave quite differently in a gasification reactor because of the unique associations of the maceral and mineral species in the coal matrix.

When the coal particle is first injected into the hot gasifier, the associated water is rapidly evolved. This drying mechanism is usually modeled as being independent of the other subsequent reactions; however, intuition says that a severe drying action could alter the particle's surface characteristics which in turn would significantly alter the later devolatilization and gasification reactions. As the dry coal particle is then rapidly heated, bound water, carbon oxides and hydrocarbon fragments are thermally cleaved from the coal's organic matrix and evolves into the surrounding gas phase. The amount and composition of this "volatile matter" are significantly controlled by the heat and mass transfer conditions in that pyrolysis/devolatilization zone. The physical severity of those devolatilization reactions, sometimes resembling mini-explosions, drastically affects the rate of the subsequent char-gasification reactions.

Today's most commercially-successful coal gasification processes completely shatter the coal's organic structure into blends of carbon monoxide and hydrogen, syngas mixtures that can be reassembled into a variety of desired gaseous and liquid products (1). Although proven to be technically and economically feasible in the present energy-market atmosphere, that destruction and reconstruction method of converting coal to useful energy and feedstock forms may not have the highest thermodynamic efficiency compared to other yet-to-be commercialized coal²conversion mechanisms. In a return to the controlled destructive distillation of the old coke-making era, research emphasis is now re-examining low-temperature, "mild gasification" methods which can skillfully carve a suite of desirable products from the coal-structure, such as specific specie blends of gaseous feedstocks and/or highly aromatic condensibles, along with specially-formed chars (2).

In order to recognize the most expedient paths to perform these selective coal-radical slicing, one must understand fully the individual pyrolysis/devolatilization reactions of that particular coal. A laminar flow reactor has some advantages in studying coal devolatilization, such as precise control of experimental conditions like the flow rate and composition of the carrier-reactant gas. Also, both the reactor temperature and particle residence time can be easily

varied to evaluate the effects of changes of the heating rate of the coal-particle. There are also disadvantages to analyzing the data from such a laminar-flow reactor system, mainly associated with the need to mathematically compute the particle temperature and then to isolate the chemical reactivity from the mass transfer resistances. Many of the original studies using laminar-flow reactors used rather high temperatures where the particle heatup time was negligible. This permitted the particles to be considered at steady-state temperature for the entire particle residence time in the reactor. However, studies of the coal devolatilization in the 650° to 1100°K range in inert or non-igniting atmospheres reveal significant time-lags before devolatilization weight-loss starts.

In this presentation, experimental weight-loss data from the devolatilization treatment of a Herrin (Illinois) No. 6 coal in a laminar-flow laboratory reactor are examined and the observed reaction behavior are used to outline criteria for a coal-pyrolysis kinetic model.

EXPERIMENTAL REACTOR SYSTEM

The concept of the laminar-flow reactor design derives from those used by Badzloch and Hawksley (3), Kobayashi (4), Nsakala et al. (5) and Agreda et al. (6). Modifications were made in the design of the coal-feed inlet and the exiting-solids collector tube to permit a smooth 0.46 gm/min flow of coal solids, to expose the solids to reactor temperatures up to 1073°K with particle residence times up about 400-500 msec, and to collect and quickly quench-cool the coal-char solids immediately as they leave the hot-zone of the reactor. This reactor system, described in detail by Wu (7) and Moslehi (8), is illustrated in Figure 1.

In this reactor system, the hot nitrogen-gas stream enters the top head of the reactor into the shell-annulus surrounding the coal-feeder tip. This gas is then directed down into the main reactor tube chamber through a flow-straightener formed from a 3.8 cm (1.5-inch) thick disk of Corning "Macor" machineable glass-ceramic through which 2.2 mm diameter holes were drilled to form a 38% voidage ratio across the primary gas flow region. The vertical reactor chamber body was formed of a nominal two-inch, Schedule 40, Type 316 stainless-steel tube twenty inches long surrounded by a tube furnace. After passing through the heated reactor zone, the solids enter the throat of the char-solids collector where a cool-flush of nitrogen flowing inward through a permeable sintered stainless-steel tube at the collector tip quickly quench-cools the solid-particle and dilutes the surrounding reactive gases. The solids are separated in mini-cyclones and the condensible and permanent gases collected for quantification and analysis. The collector assembly tube was designed with a slip-joint around its outside diameter so that the uppermost tip of the collector could be positioned at any desired distance below the coal-inlet feeder tip. Thus, the coal particle reaction path-length, which determines the particle residence time, can be varied from almost zero to more than 50 cm.

The Herrin (Illinois) No. 6 coal used in the experiments was extracted from a west-central Illinois underground mine and had a dry-analysis of 43.3% volatile matter, 9.8% ash and 46.9% fixed carbon, along with a 4.2% total sulfur content. The coal was vacuum-dried and ground to an average particle diameter of about 75 micrometers before being fed to the reactor. The operating conditions of the reactor during the processing of this coal are listed in Table 1.

EXPERIMENTAL RESULTS AND DISCUSSION

The pyrolysis reactions were examined at three reactor temperatures; 450°, 600° and 800°C; and at three particle flow path lengths; 10, 20 and 30 cm. The

total residence times of the coal-particles, computed using the reactor operating conditions existing at these nine temperature-length combinations, are listed in Table 1, the values ranging from 137 to 473 msec. The overall weight-loss data from these experiments, computed by an ash-content balance and expressed on a dry ash-free basis, are shown in Figure 2. The reasoning and procedures of all the computational analyses have been detailed by Wu (7) and Moslehi (8).

It can be seen in Figure 2 that for a given temperature, the weight loss increases with time almost exponentially, approaching a maximum value. This maximum weight loss value is definitely a function of temperature, with a value in the upper 40% (daf weight loss) approached at 600°C, while the maximum weight loss at 800°C is in the upper 50% range.

Although the five-stage succession of devolatilization reactions detailed by Suuberg et al. (9) is probably the most chemically realistic, the single-reaction first order decomposition model discussed by Howard (10) can be utilized in approximating the coal's devolatilization behavior for quick comparison with those described in previous literature-reported studies. This model is stated as;

$$dW/dt = k (W^* - W) \quad 1).$$

where W represents the weight-loss of the coal-particle (expressed on a dry ash-free basis) and W^* is the weight loss after an infinite exposure time at the reaction temperature, gas flow rate and other operating conditions. Badzioch and Hawksley (3) and other investigators realized that there was negligible weight loss until the dry coal particle was heated to about the 300^o-to-500^oC temperature range where the weight loss reactions became significant. They incorporated a particle heating time into their model;

$$\text{Total Time} = \text{Heatup Time} + \text{Reaction Time.} \quad 2).$$

In order to simplify the mathematics, they assumed there to be no reactions taking place during this heatup time, even though the particle would be heating slowly through the entire devolatilization temperature range up to the steady-state temperature of the reactor.

Using the relationships derived by Kobayashi (4) in a mathematical analysis of the temperature and velocity flow in a similar laminar-flow reactor, which were modified and used by Agreda et al. (6) and Felder and coworkers (11) in their studies, particle heatup times were computed to be in the range of 24 to 27 msec for the three experimental reactor temperatures. The values of the pseudo rate constant, k , yielded a reasonably straight line on an Arrhenius plot. This experimental data correlates by the expression;

$$k = k_0 \exp (-E/RT) \quad 3).$$

with the pre-exponential factor, k_0 , being equal to 16035 sec⁻¹ and the apparent activation energy, E , being equal to 68.12 kJ/mole (16.27 kcal/mole). This activation energy value compares quite well with the results found by Felder et al. (11) who, when devolatilizing a western Kentucky No. 11 coal in a similar reactor system, found the value of the apparent activation energy to be 80 kJ/mole (19.12 kcal/mole).

For use as a comparison with the experimental results of this study as shown in Figure 2, the devolatilization weight loss data reported by Felder et al. (11) for the western Kentucky Seam No. 11 coal is plotted in Figure 3. It

should be noted that the western Kentucky coal Seam No. 11 is believed to have been deposited in the same geological time-period as the Herrin (Illinois) No. 6 seam. The lines sketched in both Figures 2 and 3 are merely to depict a trend-connection of the points, not to suggest a specifically derived model path.

The 450°C and the 600°C weight-loss lines of Figure 2, along with the 600°C line of Figure 3, demonstrate that there is a definite effect of reactor temperature on the heating time of the particle. The mathematical analysis of Kobayashi (4) used to approximate the particle heatup time in this study was originally derived for coal devolatilization at much higher reactor temperatures than those of these experiments. Both the 800°C lines in Figure 2 and 3 could approach zero reaction within the 20-30 msec range predicted by the Kobayashi relationship. At the lower temperatures, however, the onset of devolatilization is much affected by reactor temperature as well as by other reactor operating conditions. The Felder et al. data for the 600°C experiments in Figure 3 indicate that no weight loss occurred for almost 200 msec, while at 600°C in this study, the reactions seem to have started before 100 msec.

Note also that reactor operating conditions, other than the temperature effect, seem to cause differences in the maximum asymptotic weight loss at each reactor temperature. In this study at 600°C, the maximumdaf weight loss was around 40%, while the 600°C line in Figure 3 was leveling in the 15% range. At 800°C the data in Figure 3 demonstrated a maximum weight loss of around 49%, which was about 1.11 times the ASTM Proximate Analysis Volatile Matter of that coal. In the study reported in this paper, the coal's weight loss after 300 msec had reached almost 60% (1.24 times the ASTM Proximate Volatile Matter) and the maximum weight-loss asymptote had not been reached.

An examination of the approached asymptotes of W^* at the various temperatures suggests the validity of the "multiple reactions" model developed by several investigators and discussed by Howard (10). In Figure 2, the 450°C and the 600°C data appear to be approaching ultimate W^* values that are very close together, while the 800°C value of W^* is more than 20% higher. The data of Felder et al. (11) in Figure 3 indicates that the maximum weight loss W^* at 800°C is almost three times larger than the value of W^* at 600°C, with weight loss curve at 700°C still increasing after 1000 msec of reaction exposure time. Suuberg et al. (9) in their listing of the five stages of devolatilization states that carbon oxides, hydrocarbons, tar and hydrogen are released in the fourth stage from 700°C to 900°C. It would be logical to suggest that the reactions occurring in this temperature range would be strongly influenced by variations in the mass and heat transfer mechanisms caused by differences between reactor operating conditions. Also, the primary volatile hydrocarbon species being evolved in this temperature range would be susceptible to secondary decomposition and/or cracking reactions. Thus, the pyrolysis reaction chain probably includes a complex mix of both parallel and successive reactions.

CONCLUSIONS

A Herrin (Illinois) No. 6 coal was devolatilized in nitrogen in a laboratory laminar flow reactor system. The reactions took place at 450°C, 600°C and 800°C for reaction residence times ranging from 130 to 480 msec at Reynolds Numbers of 235-308. The experimental data can be reasonably approximated by a single reaction decomposition model; $dW/dt = k(W^* - W)$; with the pre-exponential found to be 16035 sec^{-1} and the apparent activation energy being equal to 68.12 kJ/mole (16.27 kcal/mole). This reactor system stimulates a rather efficient reaction as evidenced by the fact that, after only 300 msec exposure at 800°C, the coal's weight loss had reached almost 60% (1.24 times the ASTM Proximate Analysis Volatile Matter) and the maximum weight-loss asymptote had not been reached.

At the lower temperatures of this experimental study, 450° through 600°C, knowledge of the particle heatup time is quite important. Estimates by previous investigators of the time-period before the "onset of devolatilization weight loss" occurs were substantially smaller than the actual experimental values observed in this study. There is considerable evidence that the particle heating rate and the flow conditions within the reactor system have a significant bearing on not only the pyrolysis rate, but also on the maximum weight loss of the coal which could be achieved at each reactor exposure temperature. Also, implications are that the overall devolatilization is both a parallel and a successive series of reactions, each influenced by the interrelated mass and heat transfer mechanisms occurring in that specific reactor system.

A predictive model useful in representing the reactive behavior of high-volatile coal at relatively low temperatures must incorporate a consideration of the very complex mix of mass and heat transfer effects. The development of such a model is the next stage of this continuing investigation.

ACKNOWLEDGMENTS

This research effort was supported by the U.S. Department of Energy through their Contract No. DE-FG22-82PC50802. The cooperative help of the SIU-C College of Engineering and Technology and the SIU-C Coal Extraction and Utilization Research Center is also gratefully acknowledged and appreciated.

REFERENCES

- (1) Courty, P., and Chaumette, P., "Syngas: A Promising Feedstock In The 'Near Future", *Energy Progress*, 7, 23-30, (March 1987).
- (2) Khan, M.R., and Kurata, T.M., "The Feasibility Of Mild Gasification Of Coal: Research Needs", Report No. DOE/METC-85/4019, Morgantown Energy Technology Center, U. S. Department Of Energy, Morgantown, West Virginia, (July 1985).
- (3) Badzioch, S., and Hawksley, G.W., "Kinetics Of Thermal Decomposition Of Pulverized Coal Particles", *Ind. Eng. Chem., Process Des. Dev.*, 9, 421, (1970).
- (4) Kobayashi, M., "Devolatilization Of Pulverized Coal At High Temperatures", Ph.D. Thesis, Department of Mechanical Engineering, Massachusetts Institute of Technology, Cambridge, Massachusetts, (1976).
- (5) Nsakala, N., Essenhigh, R.N., and Walker, P.L., Jr., "Studies On Coal Reactivity: Kinetics Of Lignite Pyrolysis In Nitrogen at 808°C", *Combustion Science and Technology*, 16, 153, (1977).
- (6) Agreda, V.H., Felder, R.M., and Ferrett, J.K., "Devolatilization Kinetics and Elemental Release In The Pyrolysis Of Pulverized Coal", EPA Report No. EPA-600/7-79-241, U.S. Environmental Protection Agency, Washington, D.C., (November 1979).
- (7) Wu, R-C.R., "Reaction Model and Standardized Test Procedure For Coal Devolatilization In A Laminar Flow Reactor", M.S. (Engineering) Thesis, Thermal and Environmental Engineering Department, Southern Illinois University, Carbondale, Illinois, (August 1984).
- (8) Moslehi, A., "Devolatilization Of An Illinois Coal In A Laminar Flow Reactor", M.S. (Engineering) Thesis, Thermal and Environmental Engineering Department, Southern Illinois University, Carbondale, Illinois, (January 1985).
- (9) Suuberg, R.M., Peters M.A., and Howard, J.B., "Product Composition And Kinetics Of Lignite Pyrolysis", *Ind. Eng. Chem., Process Des. Dev.*, 17, 37, (1978).

- (10) Howard, J.B., "Chapter 12: Fundamentals Of Coal Pyrolysis and Hydropyrolysis", in "Chemistry Of Coal Utilization, Second Supplementary Volume", M.A. Elliott, Editor, John Wiley & Sons, New York, pp. 727-739, (1981).
- (11) Felder, R.M., Kau, C.-C., Ferrell, J.K., and Ganesan, S., "Rates And Equilibria Of Devolatilization And Trace Element Evolution In Coal Pyrolysis", Report No. EPA 600/7-82-027, U.S. Environmental Protection Agency, Washington, D.C., (April 1982).

TABLE 1
EXPERIMENTAL REACTOR OPERATING CONDITIONS

Reactor Temperature	REACTOR TEMPERATURE		
	723 K (450°C)	873 K (600°C)	1073 K (800°C)
Dried Coal Feed Rate (gm/min)	0.46	0.46	0.46
Nitrogen Gas Flow Rate (L/min at 20°C, 1 atm)			
Main Gas Stream	20	20	20
Solids-Carrier Gas Stream	1	1	1
Combined Gas Velocity, (m/sec)	0.412	0.497	0.574
Total Gas Flow Reynolds Number	308	274	235
Coal-Solids Residence Time, msec			
Particle Flow Path Length			
10 cm	186	155	137
20 cm	336	280	227
30 cm	473	393	318

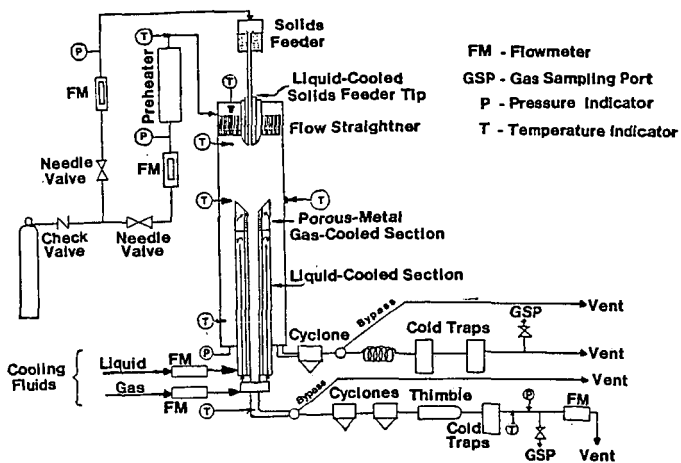


Figure 1. Experimental Laminar-Flow Reactor System

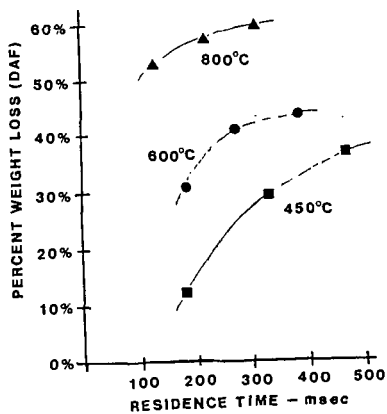


Figure 2. Weight-Loss (DAF) Versus Time, Herrin (Illinois) No. 6 Coal, This Study

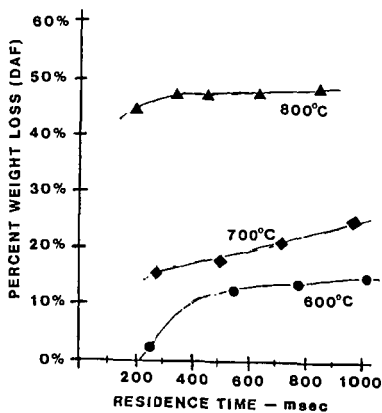


Figure 3. Weight-Loss (DAF) Versus Time, Western Kentucky No. 11 Coal, Felder et al. (Reference 11)

The Role of Coal Devolatilization in Comprehensive Combustion Models

B. Scott Brewster, Larry L. Baxter, and L. Douglas Smoot

Brigham Young University, Provo, UT 84602

Introduction

Pulverized coal combustion is a complex interaction of several processes, including particle dispersion, gas-phase mixing, particle heatup and mass transfer, particle and gas reactions, recirculating and swirling fluid mechanics, radiative heat transfer, mineral matter phase transformations, and pollutant formation and destruction. Comprehensive models which include submodels for many of these processes have been developed by several investigators (1-4) to predict local conditions inside combustors. This paper focuses on the role of coal devolatilization submodels in such predictions.

Previously reported studies of the effects of devolatilization kinetics on overall combustor characteristics have demonstrated that combustion efficiency, flame front location, and fluid dynamical structure, are all sensitive to devolatilization rate over the range of published values (5). Similar effects were noted in this study. Based on these findings, the rate of mass evolution during devolatilization is considered to be important to flowfield and particle predictions. However, devolatilization rates are currently not well established, and this paper will not address this issue further.

The objectives of this paper are (1) to present theoretical results from an investigation of several thermal effects on devolatilization for single particles and in a comprehensive predictive model and (2) to illustrate the importance of considering chemistry/turbulence interactions when extending the model to allow for variable composition of the coal volatiles. The comprehensive model that was used is PCGC-2, Pulverized Coal Gasification or Combustion-2 Dimensional (axisymmetric). Thermal effects that were investigated include variable particle heat capacity, particle emissivity, heat of reaction during devolatilization, and volatiles heating value.

Variable Particle Heat Capacity

Merrick (6) suggested the following function for coal heat capacity:

$$c_v = \left(\frac{R}{a}\right) \left[g_1 \left(\frac{380}{T} \right) + 2g_1 \left(\frac{1800}{T} \right) \right] \quad 1)$$

where g_1 is given by

$$g_1(z) = \frac{e^z}{\left[\frac{(e^z - 1)}{z} \right]^2} \quad 2)$$

These equations can be used for both coal and char and predict a monotonic increase in c_v with temperature. However, because composition varies with time, the increase in c_v for a heating and reacting particle may not be monotonic due to changes in average atomic weight (6). The high temperature limit for Equation 1 is $3R/a$, which agrees with principles of physical chemistry.

Using Equation 1, Merrick obtained agreement between predicted and experimental values within about 10% over the temperature range of the available data (0-300°C) for various coal ranks (15-35% volatile matter). Graphite and char heat capacities were correlated within 5% over the range 0-800°C.

Calculations were carried out for single particles of 40 and 100 microns and for coal-water-slurry to test the effect of variable heat capacity on particle temperature and devolatilization rate. Particle heat capacities were calculated as the weighted sum of the heat capacities for raw coal, char, and ash. Gas temperature was assumed constant at 2100 K. Constant heat capacity cases were calculated using heat capacities calculated at 350 K and 525 K for the coal and char components, respectively. The two-equation model was used for devolatilization, with coefficients suggested by Ubhayakar et al. (Z). The average atomic weights for the coal and char were assumed to be 8.18 and 12.0, respectively, with the latter corresponding to pure carbon. The heat capacity of ash was taken to be (6)

$$c_v = 593.3 + 0.586 T$$

3)

The heat capacity of the particles at constant pressure was assumed equal to the heat capacity at constant volume. Radiative heat transfer and particle blowing were taken into account. However, oxidation was neglected to more clearly illustrate the effects of heat capacity.

Profiles of temperature and devolatilization rate for the 100-micron particles are shown in Figure 1. The gas temperature is also shown for comparison. Calculations for the 40-micron coal particles and coal-water slurry droplets showed similar effects of variable heat capacity during particle heatup. The initial heatup rate for the 100- μ m particles is approximately 1.6×10^5 K/s for both constant and variable c_p . As particle temperature increases, heatup of the particle with variable c_p is retarded by the increasing value of c_p , as shown in Figure 1a, resulting in a temperature difference between the two particles of as much as 500 degrees K. This temperature lag results in a 50 percent increase in the time required for particle ignition and a slight decrease in the devolatilization rate, as shown in Figure 1b. The slower heatup rate during devolatilization allows a greater portion of the particle to devolatilize via the low-temperature reaction, thus giving an ultimate volatiles yield that is approximately 5 percent lower than for the particle with constant c_p .

As shown in Figure 1a, the heatup rate decreases markedly during devolatilization, due to the blowing effect. This effect was similarly predicted by Ubhayakar and coworkers (Z). The asymptotic temperature of both particles is approximately 200 degrees less than the gas temperature, due to radiative heat losses to the walls of the reactor, which were assumed to have a temperature of 1000 K.

Calculations were also performed with the comprehensive code (PCGC-2) for particles with constant and variable heat capacity. Contour plots of temperature for the constant and variable c_p cases are shown in Figures 2a and 2b, respectively. As shown, the temperature fields are similar, except that the temperature is somewhat lower in the variable c_p case. This can be seen by noting that the isotherms in Figure 2b are generally shifted toward the exit and centerline. The lower gas temperature was predominantly a result of the decrease in volatile yield from the coal. The delay in particle ignition caused by variable c_p is also apparent in Figure 2b on the centerline at the inlet.

The effect of variable heat capacity on total burnout is shown in Figure 3. The curve for variable c_p is shifted to the right, resulting in a decrease of approximately 3 percent in particle burnout at the exit of the reactor. This effect is consistent with the delayed ignition and slightly slower devolatilization rate observed in the single particle calculations. Interestingly, the decrease in burnout is approximately equal to the decrease in ultimate volatiles yield predicted for the single particles, even though particle oxidation was not ignored in the comprehensive predictions.

Particle Emissivity

Total emissivities for coal particles have been reported with large variation, as summarized by Solomon et al. (8). Measurements by Brewster and Kunitomo (9) for micron-sized particles suggest that previous determinations of the imaginary part of the index of refraction for coal may be too high by an order of magnitude. If so, the calculated coal

emissivity for these particles based on previous values may also be too high. However, the experimental work of Baxter et al. (10) indicates that the effective emissivity of 100-micron coal particles of several ranks of coal at low temperatures is probably not less than 0.7.

To investigate the sensitivity of devolatilization to coal emissivity, calculations were again performed for single particles and with the comprehensive code. For the single particle cases, emissivity was varied between 0.9 and 0.1. In the comprehensive code calculations, emissivity was varied from 0.9 to 0.3. The wall temperature was 1250 K in the former and 1000 K in the latter.

Little effect of emissivity was noted in either set of calculations. The high gas temperature in the single particle calculations made convection/conduction the principal mode of heat transfer. In the comprehensive code simulations, the secondary air was swirled (swirl no. = 2), and the flow field was recirculating. Thus the particles were heated largely by contact with hot recirculating gases and not by radiation. In larger furnaces, or in reactors where the particles do not immediately contact hot gases, radiation may contribute significantly to particle heating, and in this case, greater sensitivity to the value of particle emissivity would be expected.

Heat of Reaction

A similar investigation was initiated on the effect of heat of reaction for devolatilization. Investigators disagree on both the magnitude and sign of the heat of reaction. Reported values range from -65.3 kJ/kg to +334 KJ/kg (6,11). Merrick (6) speculates that the source of the disagreement is related to the effect of variable heat capacity. The heat of reaction probably varies with coal type. However, our preliminary conclusions are that devolatilization calculations are insensitive to this parameter, which agrees with the conclusion of Solomon and Serio (11). Investigation of the effect of heat of reaction is continuing.

Volatiles Heating Value

The heating value of the coal volatiles must be known in order to calculate the energy released by gas-phase reactions. This heating value is a function of volatiles composition, which is a function of burnout. However, in comprehensive combustion simulations that treat the effects of chemistry/turbulence interactions (discussed in the next section), both heating value and composition of the volatiles are often assumed constant.

The effect of variable heating value was not tested in single particle calculations, because gas-phase reactions were not included in this model. The sensitivity of the comprehensive code to changing volatiles heating value was tested in an approximate manner by increasing the heat of formation of the coal. Since the volatiles enthalpy is calculated from a particle heat balance, and over 80 percent of the total particle mass loss was due to devolatilization, increasing the heat of formation of the coal effectively increased the volatiles heating value. A value was chosen such that the adiabatic flame temperature of the coal at a stoichiometric ratio of unity was increased by about 200 K. Since the simulations were performed for fuel-lean (combustion) conditions, the actual gas temperatures increased by 50-75 K.

The results of this investigation are shown in Figures 2 and 3. As shown in Figure 2c, the gas temperatures are seen to be higher with the increased heat of formation of coal. Otherwise the temperature fields are quite similar. The higher temperatures are due to a combination of higher heating value and greater volatiles yield. The latter effect dominates everywhere except in the near-burner region. The higher temperature significantly affects coal burnout, as shown in Figure 3, with a large portion of the impact coming from the volatile yield in the early regions of the reactor. The magnitude of the variation of the offgas heating value was arbitrary in this case, but is regarded as representative of actual coals and possibly conservative.

Volatiles Composition

The variation of char and coal offgas composition with burnout has been correlated by both simple and complex reaction schemes (12-14). Accounting for this variation is not difficult for the particles. However, dealing with this variable composition and its interplay with gas phase turbulent mixing and kinetics is both complex and computationally expensive.

The successful prediction of turbulent and mean flow properties is a difficult proposition in typical combustion environments (15). Although reasonable success has been achieved for some simple flows, the complexity of reacting, swirling, turbulent flows often exceeds the capability of even sophisticated turbulence models. The added complexity of chemical effects on these predictions and the effect of turbulence on the mean reaction rates compounds the problem. Indeed, combustion investigators have identified this problem as one of the critical needs of combustion research (16).

Several approaches to the problem have been proposed. Some of these were recently reviewed and compared to data by Smith and Fletcher (17). The approach used in the current paper is the statistical, coal gas mixture fraction model. The detailed theory and assumptions of this model are given elsewhere (1). Only a brief discussion is given here.

The statistical, coal gas mixture fraction model involves convolving instantaneous properties over the turbulent statistics of the mixture to get time-mean properties. The statistics of the mixture is represented by the multivariate probability density function of a number of independent progress variables. The instantaneous mixture properties must all be represented as functions of only these progress variables.

The current code PCGC-2 allows for two progress variables. One progress variable is typically used for the inlet gas mixture fraction and the other is used for the coal offgas mixture fraction. The coal offgas composition is therefore assumed constant. Chemical kinetics are assumed fast for major gas species (intermixing of fuel and oxidizer is rate-limiting), so that the mixture is in local instantaneous equilibrium, and local properties depend only on the local elemental composition and enthalpy. With the two mixture fractions, the local composition is specified. Enthalpy fluctuations are assumed to be correlated with fluctuations in the stoichiometric ratio, as given by the two mixture fractions. Time-mean properties are therefore calculated by a double integral over the joint probability density function of the two mixture fractions. The evaluation of this integral consumes a significantly greater fraction of the computational time than any other single task in the code, even though a table of equilibrium properties is used to minimize the time spent performing equilibrium calculations.

Additional progress variables are required if coal offgas composition is to be allowed to vary. Each group of elements that are evolved from the coal must be tracked independently. Each additional progress variable for which the statistical variance is taken into account will increase the computational burden of this approach substantially. An investigation of the importance of variable coal offgas composition in a comprehensive code that treats chemistry/turbulence interactions has never been reported. Such an investigation would determine the extent to which such effects should be taken into account. It may be possible to ignore the turbulent fluctuations of some or all progress variables when allowing offgas composition to vary. If so, the computational burden would be reduced significantly.

The computational effort involved with the convolutions is not the only significant consideration in treating large numbers of progress variables. A multi-variate probability density function is required to perform the convolution. However, transport equations are typically written to describe individual probability density functions. To the extent that the fluctuations in the mixture fractions are independent of each other, the multi-variate pdf's will be equal to the product of the individual pdf's. However, as the number of progress variables increases, this independence will be difficult to maintain. Predicting the correlation coefficients will be difficult and the relevance of the model could be compromised.

A study of the impact of turbulent fluctuations on overall predictions was conducted to evaluate their importance. In this study, the fluctuations were either arbitrarily neglected or included, and the results of the comprehensive predictions under these assumptions were

compared. Similar results are shown by Smith and Fletcher (17). These results are an extension of their work, focusing on the effect of the coal offgas fluctuations. Figures 4, 5, and 6 show the results of ignoring turbulent fluctuations in the coal gas mixture fraction on gas temperature, total particle burnout, and centerline NO_x concentration. The coal gas mixture fraction η represents the degree of mixing between the coal volatiles and the inlet gas. As expected, neglecting the fluctuations in inlet gas mixture fraction had little effect on the calculations, since both the primary and secondary streams were air at 300 and 589 K, respectively.

The effect of ignoring the fluctuations in η on gas temperature can be seen by comparing Figures 2a and 4. Ignoring the fluctuations caused a high temperature ridge at the location of mixing between the primary and secondary streams, as can be seen by the higher concentration of isotherms in Figure 4. Taking the fluctuations into account smoothed the high temperature peaks. Similar observations were made by Smith and Fletcher (17) when they ignored turbulent fluctuations in both mixture fractions. Because the rate of mixing of fuel and oxidizer is reduced when turbulent fluctuations are ignored, the particle burnout is lowered as shown in Figure 5.

The above results were obtained assuming that the mixing is rate-limiting. The kinetics of NO_x formation and destruction are of the same order of magnitude as the turbulent mixing rates. Therefore, both mixing and kinetic considerations must be made to predict NO_x concentrations. The model used to do so has been previously reported (18) and incorporated as a submodel in PCGC-2.

Figure 6 shows the effect of the fluctuations on pollutant predictions. In Figure 6a, turbulent fluctuations were ignored both in the calculation of major species, and in the calculation of the pollutant species, which are decoupled from the calculation of major species. In Figure 6b, turbulent fluctuations were taken into account for both calculations. As shown, the predicted NO levels are quite sensitive to rigorous accounting for the effects of turbulence on chemistry. When turbulent fluctuations are taken into account, oxygen from the secondary mixes more rapidly with the primary, and more NO_x is formed. Although data were not available for comparison with this calculation, previously reported calculations have shown that solutions taking the turbulence into account agree more closely with data (18).

Conclusions

Coal devolatilization is typically responsible for flame ignition and the ignition point and volatile yield of the devolatilization reactions have large impacts on overall combustion characteristics.

The temperature and composition dependence of particle heat capacity alters comprehensive code predictions of particle temperature, particle ignition, particle burnout, gas ignition and combustion efficiency. The effect is predominantly linked to the predicted ignition point of the coal and the extent of devolatilization.

For typical operating conditions of entrained-flow reactors (cold walls, hot gas), the value of coal particle emissivity does not significantly affect comprehensive code predictions. Preliminary results indicate that predictions are also insensitive to heat of devolatilization, but further investigation of this effect is needed. These conclusions may be different in situations with less dominant conductive/convective heat transfer.

The heating value of the coal offgas affects coal burnout and, to a lesser extent, gas temperature. This effect is attributed to the volatile yield of the coal under different heating conditions. Correlations of offgas heating value with particle burnout may improve comprehensive code predictions.

Turbulent fluctuations have an important impact on the mean reaction rate of coal offgas with the gas mixture. Further investigation of the importance of variable coal offgas composition in comprehensive codes and the importance of including the effect of turbulent fluctuations is proceeding.

Acknowledgements

This study was conducted principally under subcontract to Advanced Fuel Research, Inc., who was under contract to the Morgantown Energy Technology Center (Contract No. DE-AC21-86MC23075). Mr. Justin Beeson is the contract officer. Some of the single particle calculations were performed by Mr. Larry Baxter while he was on leave at Sandia National Laboratories in Livermore, California.

List of Symbols

a	average atomic weight of coal or char (kg/kg-mol)
c_v	constant volume heat capacity (J/kg-K)
g_1	function defined by Equation 2
R	universal gas constant (8314.4 J/kg-mol/K)
T	temperature (K)
z	parameter in Equation 2

Literature Cited

1. Smoot, L.D. and P.J. Smith, *Coal Combustion and Gasification*, Plenum Press, New York (1985).
2. Lockwood, F.C. and A.S. Abbas, "Prediction of a Corner-Fired Utility Boiler," *21st Symposium (International) on Combustion*, The Combustion Institute, Munich, West Germany, August 3-8 (1986).
3. Boyd, R.K. and J.H. Kent, "Three-Dimensional Furnace Computer Modelling," *21st Symposium (International) on Combustion*, The Combustion Institute, Munich, West Germany, August 3-8 (1986).
4. Truelove, J.S., "Prediction of the Near-Burner Flow and Combustion in Swirling Pulverized-Coal Flames," *21st Symposium (International) on Combustion*, The Combustion Institute, Munich, West Germany, August 3-8 (1986).
5. Fletcher, T.H., "Sensitivity of Combustion Calculations to Devolatilization Rate Expressions," Sandia National Laboratories, SAND85-8854 (1985).
6. Merrick, D., "Mathematical Models of the Thermal Decomposition of Coal. 2. Specific Heats and Heats of Reaction," *Fuel*, **62**, 540-6 (1983).
7. Ubhayakar, S.K., D.B. Stickler, C.W. von Rosenberg, Jr., and R.E. Gannon, "Rapid Devolatilization of Pulverized Coal in Hot Combustion Gases," *16th Symposium (International) on Combustion*, The Combustion Institute, Pittsburgh, Pennsylvania, 427-36(1977).
8. Solomon, P.R., M.A. Serio, R.M. Carangelo, and J.R. Markham, "Very Rapid Coal Pyrolysis," *Fuel*, **65**, 182-94, (1986).
9. Brewster, M.Q. and T. Kunitomo, "The Optical Constants of Coal, Char, and Limestone," *J. Heat Trans.*, **106**, 678-83, (1984).
10. Baxter, L.D., D.K. Ottesen, and T.H. Fletcher, "Spectral Emission Characteristics of Coal Particles," Western States Section/The Combustion Institute, 1987 Spring Meeting, Provo, Utah, April 6-7 (1987).
11. Solomon, P.R. and M.A. Serio, "Evaluation of Coal Pyrolysis Kinetics," NATO Workshop on "Fundamentals of Physical-Chemistry of Pulverized Combustion," Les Arcs, France, July 28-August 1 (1986).
12. Smoot, L.D., P.O. Hedman and P.J. Smith, "Mixing and Kinetic Processes in Pulverized Coal Combustors, User's Manual for a Computer Program for 1-Dimensional Coal Combustion or Gasification (1-DICOG)," Final Report Volume II prepared for EPRI, Contract No. 364-1-3, (1979).
13. Niksa, S. and A.R. Kerstein, "The Distributed-Energy Chain Model for Rapid Coal Devolatilization Kinetics. Part I: Formulation," *Combustion and Flame*, **66**, 95-109 (1986).

14. Serio, M.A., D.G. Hamblen, J.R. Markham, and P.R. Solomon, "Kinetics of Volatile Product Evolution in Coal Pyrolysis: Experiment and Theory," *Energy & Fuels*, **1**, 138-152 (1987).
15. Sloan, D.G., P.J. Smith, and L.D. Smoot, "Modeling of Swirl in Turbulent Flow Systems," *Prog. Energy Comb. Sci.*, **12**, 163-250 (1986).
16. Smoot, L.D. and S.C. Hill, "Critical Requirements in Combustion Research," *Prog. Energy Comb. Sci.*, **9**, 77-103 (1983).
17. Smith, P.J. and T.H. Fletcher, "A Study of Two Chemical Reaction Models in Turbulent Coal Combustion," Winter Annual ASME Meeting, Anaheim, AMD-Vol. 81, December 7-12 (1986).
18. Hill, S.C., L.D. Smoot, and P.J. Smith, "Prediction of Nitrogen Oxide Formation in Turbulent Coal Flames," *Twentieth Symposium (International) on Combustion*, The Combustion Institute, 1391-1400 (1984).
19. Smoot, L.D., P.O. Hedman, and P.J. Smith, "Pulverized-Coal Combustion Research at Brigham Young University," *Prog. Energy Combust. Sci.*, **10**, 359-441 (1984).

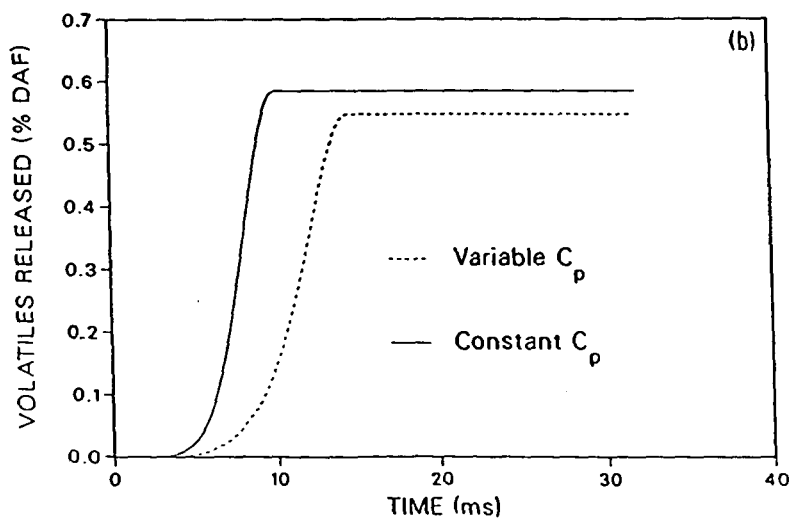
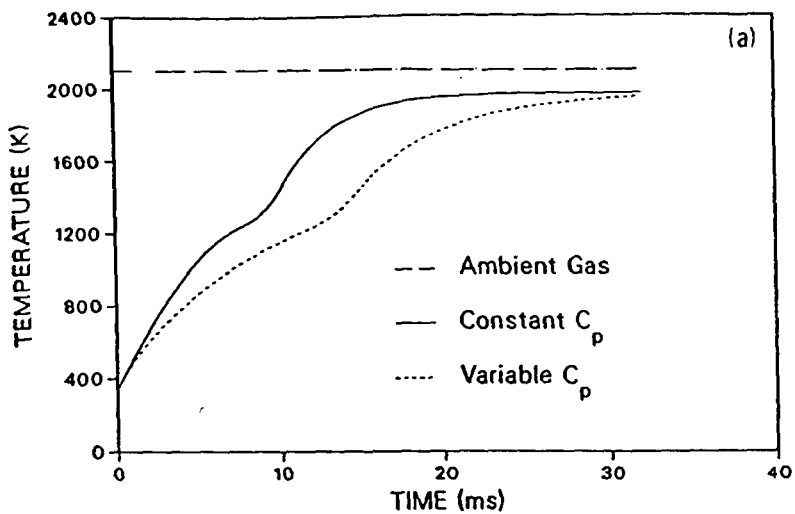


Figure 1. Variations of (a) particle temperature and (b) mass loss when different particle heat capacity formulations are used. The variable C_p case uses the correlation of Merrick (6).

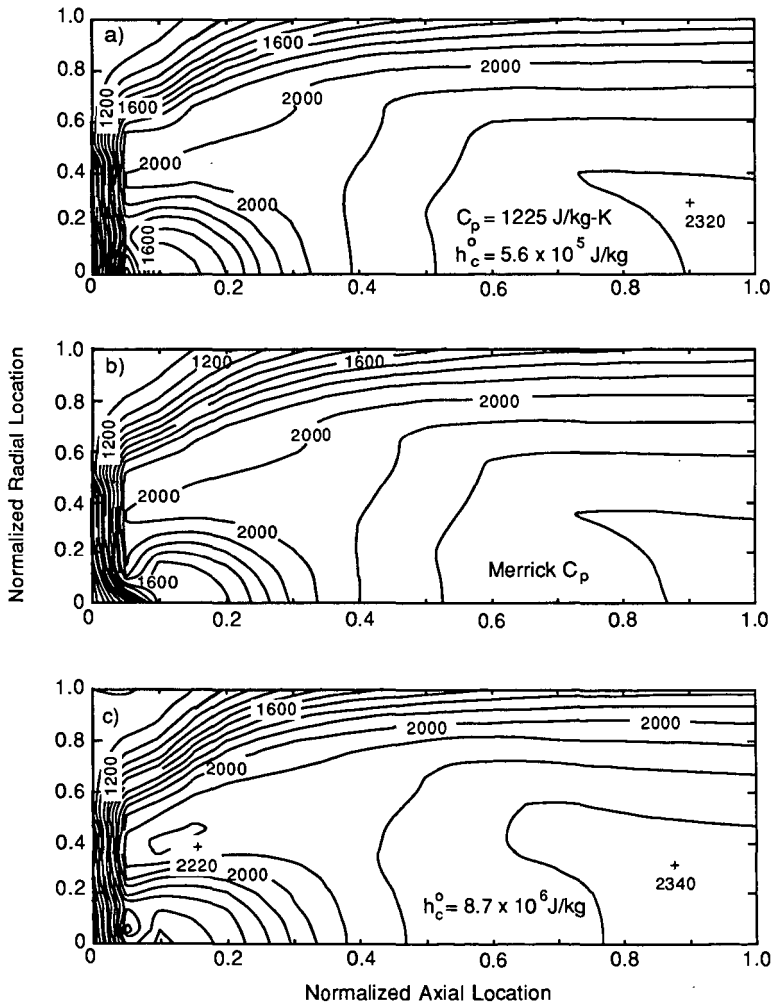


Figure 2. Contour plots of temperature for (a) constant particle heat capacity, (b) Merrick variable heat capacity, and (c) increased heat of formation of coal (h_c^o).

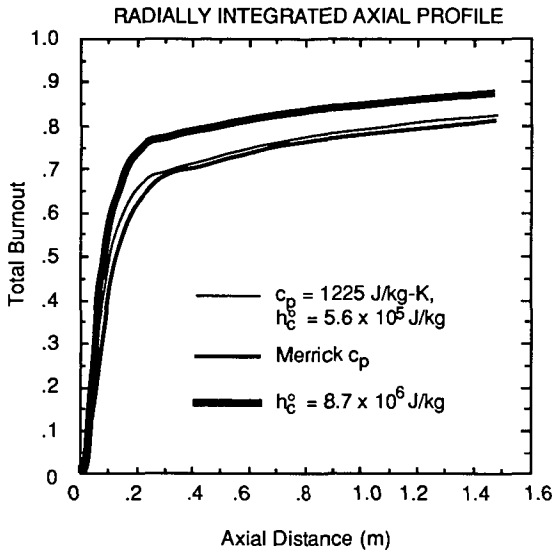


Figure 3. Effect of variable heat capacity and increased volatiles heating value on total particle burnout

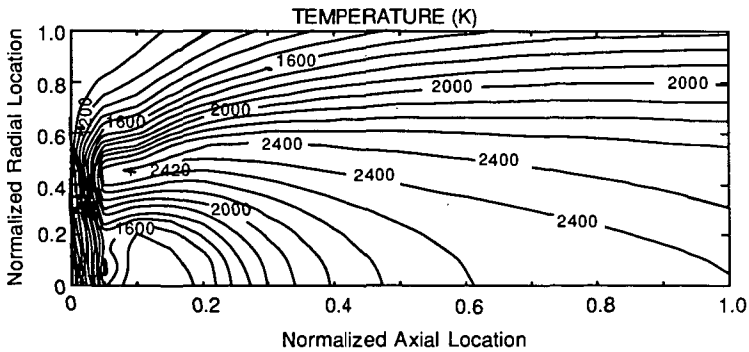


Figure 4. Gas temperature isotherms predicted when fluctuations in coal gas mixture fraction are neglected.

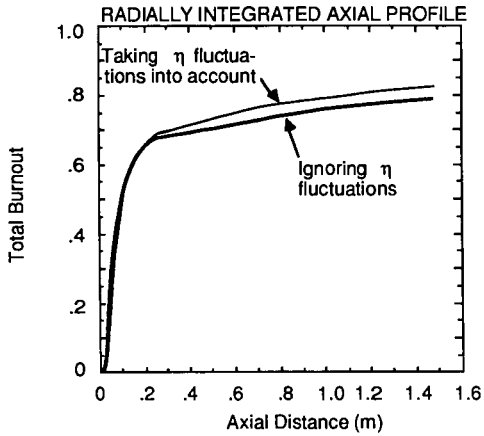


Figure 5. Effect of neglecting fluctuations in coal gas mixture fraction on total particle burnout.

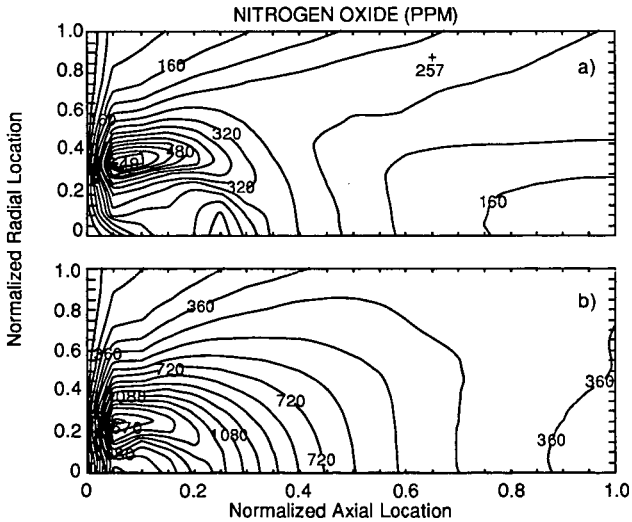


Figure 6. Predicted NO concentration (a) neglecting turbulent fluctuations of coal gas mixture fraction and (b) taking fluctuations into account.